Semi-decadal transformations in geomorphology and landcover of a mixed-energy barrier island complex in North Carolina

By Isaac G. Benaka

Dr. David W. Johnston, Advisor

April 26, 2024

Masters project submitted in partial fulfillment of the requirements for the Master of Environmental Management degree in the Nicholas School of the Environment of Duke University

Executive Summary

Barrier islands, which cover the majority of the Atlantic coastline in North America, are highly valued and dynamic coastal landforms. Serving as natural protective barriers, these islands shield inland areas and critical infrastructure from storms and wave energy while providing vital habitats for diverse ecosystems that deliver key ecosystem services. With increases in storm frequency and sea level rise caused by climate change, these islands are becoming increasingly susceptible to change, making the understanding of their dynamics crucial for their preservation and the protection of the ecosystems and human communities they support.

Research on barrier islands has predominantly focused on those facing the open ocean, with less attention given to the fetch-limited barrier islands (FLBIs) located in lagoons or sounds behind these ocean-facing islands. FLBIs are generally associated with minimal geomorphological changes under predominant conditions due to their sheltered nature. However, they can be highly susceptible to erosion during high-energy storm events, with slow morphological recovery due to the reduced movement of sediment by low wave energy in quiescent conditions.

The Rachel Carson Reserve (RCR), located within the Inner Banks of North Carolina, is a complex of inlet FLBIs that contains diverse ecosystems and acts as a barrier to storm impacts for the town of Beaufort, NC. Bird Shoal, one of three islands in the RCR, is situated directly landward of Beaufort Inlet and serves as a frontline of defense from storms. Recent scientific focus on Bird Shoal revealed significant geomorphological developments that indicate the island's departure from FLBI status and challenge the FLBI model. Specifically, Bird Shoal exhibited dynamic morphological changes outside of a storm event, while FLBIs are typically expected to exhibit minimal changes under predominant wave conditions. These observations coincided with significant widening of the Beaufort Inlet, which indicates a shift in the wave dynamics affecting the RCR.

We conducted a mapping survey of the RCR using small unoccupied aircraft systems (sUAS) and compared the data with other remotely-sensed datasets to measure how the topography and shorelines of the Reserve changed from 2017 to 2023, with a specific focus on Bird Shoal. Our synoptic analysis demonstrated both erosion and accretion to Bird Shoal from 2018 to 2023. While Bird Shoal grew in area and volume, the majority of its shoreline experienced landward migration. The dynamic morphology of Bird Shoal may be caused by altered wave dynamics influenced by the widening of the Beaufort Inlet. Our study's observed morphological changes to Bird Shoal and the potential wave dynamics at play suggest that the island deviates from the FLBI model. Additionally, the impacts of observed morphological changes were visible in a habitat change analysis, which indicated patterns of ecological succession within the RCR as a whole. For example, overwash from the migration of Bird Shoal appeared to provide a suitable platform for marsh growth.

The observed morphological and habitat changes provide crucial insights into the future evolution of the RCR and inform strategic management approaches. Continued sea level rise will likely drive increased overwash and landward migration of Bird Shoal, reshaping the Reserve's intertidal areas. The growth in dune width and elevation on Bird Shoal suggest increased sediment trapping capabilities, potentially strengthening the island's role as a coastal barrier. However, the vulnerability of the dunes to overwash remains a concern. Implementing management strategies such as planting dune-stabilizing vegetation could mitigate this risk. Continued monitoring of both morphological and habitat changes is essential to understand the evolving dynamics of inlet barrier islands and support the effective management of the Rachel Carson Reserve.

Table of Contents

Introduction

Barrier islands, which cover roughly 10% of the world's ocean-facing shorelines and 78% of the North American Atlantic coastline, are highly dynamic and valued coastal landforms (Stutz and Pilkey, 2011). Barrier islands play a crucial role in protecting inland areas, important human infrastructure, and delicate estuarine ecosystems from storm surges and waves, serving as a form of storm defense (Fritz et al., 2007; Feagin et al., 2010; Anderson et al., 2016; Arkema et al., 2013). Barrier islands not only provide habitat for unique, diverse, and productive ecosystems, but also deliver crucial ecosystem services (Barbier et al., 2008; Feagin et al., 2010; Gedan et al., 2011; Zhang et al., 2012; Mariotti and Hein, 2022). Through this century, barrier islands will be increasingly vulnerable to destabilization through greater intensity and frequency of storms (Paerl et al., 2019), and accelerating sea level rise (Valle-Levinson et al., 2017; Temmerman et al., 2013). Given these threats and the services that barrier islands provide, understanding their dynamics is crucial for their preservation and the protection of the ecosystems and human communities they safeguard.

Barrier island research has mainly focused on open-ocean-facing islands, while island systems that form in the lagoons or sounds behind ocean-facing barrier islands are much less studied. First characterized as fetch-limited barrier islands (FLBI) by Pilkey et al. (2009), these island systems are more numerous than their ocean-facing counterparts and can be found on nearly every continent. While few FLBIs are inhabited by humans, they are commonly located along the edges of estuaries—popular areas for coastal development that are experiencing increases in population growth (Neumann et al., 2015). Similar to ocean-facing barrier islands, FLBIs safeguard communities along estuarine shorelines as well as habitats behind barriers, such as salt marshes, mangroves, and oyster reefs, by reducing wave energy and preventing erosion (Feagin et al., 2010).

As their name would suggest, the shorelines of fetch-limited barrier islands typically experience locally generated wind-driven waves with less than 0.25 m of wave height (Pilkey et al., 2009). As a result, geomorphological changes to FLBIs can be minimal outside of storm events when high energy high fetch waves induce erosion and overwash (Pilkey et al., 2009; Jackson et al., 2002). FLBIs tend to recover more slowly from storms than their ocean-facing counterparts following a return to low-energy local waves, which hinder the movement of sediment from offshore bars back to eroded foreshore sections of the island (Nordstrom, 1980; Suanez et al., 2012; Baustian and Mendelssohn, 2015; Houser et al., 2015). Consequently, these islands are especially susceptible to transgression, breaching, and drowning (Jackson et al., 2002).

Inlet barrier islands, considered a subset of FLBIs by Pilkey et al. (2009), form landward behind inlets of ocean-facing barrier islands, as shoals from their flood tidal deltas become colonized by saltmarsh or move onto existing marsh platforms (Seymour et al., 2019). Marsh vegetation growth and succession traps sediment, allowing for "vertical accretion to supratidal elevations" and eventually "the formation of aeolian dunes (>10 m high)" (Seymour et al., 2019). As their associated inlet moves or closes, inlet barrier islands can migrate, changing both the location and the amount of sediment delivered by the nearby flood tidal delta (Pilkey et al., 2009). Despite being classified generally as FLBIs, some inlet barrier islands appear to not fully conform to the FLBI model put forth in Pilkey et al. (2009) because they can be exposed to oceanic waves and display considerable post-storm recovery despite being sheltered by ocean-facing islands (Smith et al., 2010; Seymour et al., 2019). Observed deviations from the FLBI model underscore the importance of studying dynamic inlet barrier islands on short time scales to capture their morphological changes.

Measuring these deviations is valuable as it refines our understanding of inlet barrier island dynamics, which is crucial for their effective management.

Study Area and Historical Context

The Inner Banks of North Carolina is a coastal region bounded by 23 ocean-facing barrier islands that consists of 4,800 km of estuarine shoreline (Crawford, 2007). The Inner Banks contain coastal communities, large areas of back barrier marsh, oyster reefs, and fetch-limited barrier islands (Crawford, 2007). The Rachel Carson Reserve (RCR), incorporated into the National Estuarine Research Reserve System (NERRS) in 1980, is a complex of three inlet barrier islands and intertidal areas, and is located south of the historic town of Beaufort, North Carolina in an area of the Inner Banks known as the Crystal Coast. For the purposes of this study, "the RCR" refers exclusively to the three main barrier islands and the estuarine area between them, although the Reserve also includes a large area of salt marsh called Middle Marsh to the east of the barrier island complex that was not a focus of this study. The RCR is separated from the town of Beaufort by Taylor Creek, a narrow dredged navigation channel that supports small boat traffic. Navigation channels also allow for boat traffic to the west of the RCR between Piver's and Radio Islands and to the east through Back Sound. The islands of the RCR are classified as inlet barrier islands because the Reserve is situated directly landward of the Beaufort Inlet. Bogue and Shackleford Banks, two ocean-facing barrier islands adjacent to Beaufort Inlet, shelter the sound where the Reserve is located from oceanic waves.

Prevailing climate conditions around the RCR are consistent with its sheltered condition. Fetch distances reach a maximum of four kilometers in Back Sound around Bird Shoal, which limits the energy of wind-driven waves generated in the sound (Seymour et al., 2019). Throughout the year, average wind speeds vary significantly, with hourly speeds ranging from 9.9 mph in August to 13.9 mph in February (National Ocean Service station BFTN7, Beaufort, NC), reflecting seasonal atmospheric patterns. The area also experiences semidiurnal tides with a mean tide range of 0.95 m (National Ocean Service station BFTN7, Beaufort, NC), defining it as a microtidal system according to classifications by Hayes (1975). The east-west orientation of the Crystal Coast makes the RCR particularly susceptible to the impacts of northward moving storms (Fear, 2008), which bring increased wind speeds and wave heights from storm surge. Between 2014 and 2020, winds from storms hitting the Crystal Coast generally approached from the east-southeast or west-southwest (Sirianni et al., 2022).

Survey maps and nautical charts dating back to 1837 identify the RCR's islands by name and demonstrate how the Reserve's geomorphology has developed since. The RCR was never settled by humans, but was used as a fishery and may have been used in some capacity by the Coree tribe of Native Americans prior to European settlement of the area (Taggart and Henderson, 1988). Anthropogenic modification of the RCR started in the early 1900s, when the U.S. Army Corps of Engineers began dredging Taylor Creek to facilitate boat traffic, depositing dredge spoils on the Reserve's islands (Evans, 1988). The RCR was also used as grazing land for livestock. In the 1980s, the RCR was incorporated into the NERRS, who manage the land in conjunction with the North Carolina Division of Coastal Management. Today, the RCR serves as a preserve for coastal ecosystems while offering recreational opportunities, and is a hotbed for coastal research (Poling, 2023; Ridge et al., 2020; Castro-Bolinaga et al., 2022; DiGiacomo et al., 2020; Selby, 2020; O'Donnell et al., 2003; Gray et al., 2018; Taggart, 2008; Seymour et al., 2019)

The Reserve covers approximately 10 km^2 and contains a variety of habitats, including maritime forest, saltmarsh platforms, seagrass beds, oyster reefs, and low-lying beaches scattered with small vegetated dunes. Because of its habitat diversity, the RCR has high animal presence compared to

areas of a similar size around the Inner Banks (Fear, 2008). Subtidal and estuarine areas serve as habitats for crustaceans, invertebrates, and shellfish reefs (Ridge et al., 2020). Marine mammals and commercially important fish species can also be found in the waters surrounding the RCR. The Reserve serves as both a stopover location for migrating birds and a seasonal nesting area, with more than 200 documented bird species frequenting its grounds (Fear, 2008). Federally threatened and endangered species can also be observed within the RCR, such as Loggerhead Sea Turtles (*Caretta caretta*) and Piping Plovers (*Charadrius melodus*). The Crystal skipper butterfly (*Atrytonopsis quinteri*), endemic to only a 50 km tract of barrier island habitat along the Crystal Coast may also use the RCR as habitat (Burns, 2015). In the 1940s, residents of Beaufort began utilizing the upland regions of the RCR for livestock grazing, including horses. As a consequence of this historical practice, approximately 40 non-native feral horses currently inhabit the Reserve. The horses primarily consume Smooth Cordgrass (*Spartina alterniflora)*, and have been shown to negatively impact biomass, seed production, percent cover, and density of *Spartina alterniflora*, thus affecting the productivity of marsh habitats (Hay and Wells, 1988).

Town Marsh, Carrot Island, and Bird Shoal comprise the three subaerial islands of the RCR. Despite its name, Town Marsh has the highest elevation of the three islands and consists of several upland areas connected by sections of emergent wetland dominated by *Spartina alterniflora*. The upland areas of Town Marsh were artificially elevated through the deposition of dredge spoils from Taylors Creek. The shore of Town Marsh has a narrow beach backed by marsh grass. Thickets and shrubs such as Groundseltree (*Baccharis halimifolia*) and Marsh Elder (*Iva frutescens*) border the emergent wetland from the upland area of the island (Fear, 2008). Town Marsh contains pockets of dense maritime forest and large shrubs including pines and oaks (Fear, 2008). The upland portion of the island also contains large areas of exposed sand colonized by graminoids such as Salt Meadow Hay (*Spartina patens*), Sea Oats (*Uniola paniculata*), and Centipede (*Eremochloa ophiuroidesand*) (Fear, 2008). An embayment, situated beside an intertidal wetland encroached upon by Bird Shoal's overwash fans, acts as the dividing line between Town Marsh and Bird Shoal. Additionally, Town Marsh is separated from Carrot Island by a tidal creek that facilitates tidal flow into the intertidal zone at the heart of the Reserve. Analysis of historical aerial and satellite imagery suggests minimal alterations to the topography of Town Marsh over the past two decades (NOAA Digitial Coast Data Access Viewer).

Carrot Island has a similar topography to Town Marsh in that it consists of multiple upland areas lined with woody shrubs that are connected to one another by wetland habitat. It also has a very narrow, and in sections, completely undeveloped beach that is backed by fringing marshland. The upland areas of Carrot Island have large woody vegetation, with the easternmost portion of the island accommodating a dense maritime forest. Carrot Island too received sediment from dredging activities that built up its upland areas. A tidal creek that separates Carrot Island from Bird Shoal runs along the southern length of the island, feeding the tidal flats of the RCR. Changes to the topography of Carrot Island have been minimal in recent years, although increased water levels due to sea level rise may have led to the loss of emergent wetland on its eastern side between 2004 and 2017, and shoreline erosion has occurred at the island's eastern end over the past two decades, likely due to wake from recreational and commercial vessels transiting between where Taylor Creek enters Back Sound (Fear, 2008; Gray et al., 2018).

Bird Shoal is the largest of the three islands (4 km long) and lies to the south of Town Marsh and Carrot Island, facing the Beaufort Inlet. Because of its position in relation to the Beaufort Inlet, Bird Shoal serves as the RCR's first line of protection from storms passing through the inlet and experiences higher wave fetch compared to the other two islands, making it a more dynamic island (Seymour et al., 2019). According to historical maps, Bird Shoal appeared as its own supratidal

landmass as early as 1888, and may have formed as a flood tidal delta from Beaufort Inlet collided with the mainland fringing marsh fronting the town of Beaufort (NCDEQ). Dredge spoils deposited on West Bird Shoal increased the elevation of this section of the island and supported dune formation along Central and East Bird Shoal, which were not directly supplemented by dredged sediment (Seymour et al., 2019). The morphology of West Bird Shoal consists of an elevated escarpment formed from dredge spoil sediments and is colonized by graminoid and large shrub vegetation. Moving east past the escarpment, West Bird Shoal transitions into a beach that includes a discontinuous dune ridge and a back barrier berm that borders a small embayment adjacent to Town Marsh. The highest dunes on the island are found on Central Bird Shoal, which also displays extensive washover terraces extending into the back barrier marsh. The eastern end of Bird Shoal is the most low-lying part of the island, and has discontinuous dunes with low elevations.

The dynamic evolution of Bird Shoal's geomorphology is evident through a series of significant changes observed since 2011, including shoreline retreat, accretion, expansion, and spit growth, reflecting the island's response to the expansion of Beaufort Inlet and other environmental factors (Seymour et al., 2019). Prior to 2011, Bird Shoal exhibited consistent landward retreat, slow split growth at the eastern end of the island, and a less embayed shoreline, conforming to the FLBI model presented in Pilkey et al. (2009) (Seymour et al., 2019). However, after 2011, geomorphological changes on Bird Shoal coinciding with widening of the Beaufort Inlet were significant and varied across different sections of the island (Seymour et al., 2019). Between 2014 and 2018, the shoreline in front of West Bird Shoal's escarpment and the escarpment itself consistently retreated landward (Seymour et al., 2019). In contrast, a 1.1 km stretch of beach just to the east of this area experienced notable accretion from 2014 to 2018, nearly doubling the width of the island in this section and coinciding with the formation of West Bird Shoal's dune ridge (Seymour et al., 2019). As Bird Shoal expanded and widened, it encroached upon and obscured the emergent wetland located between itself and Town Marsh and Carrot Island (Gray et al., 2018). At the same time, increased elevations on the landward side of Bird Shoal driven by overwash fans and aeolian transport provided suitable habitat for colonies of sparse saltmarsh vegetation where they were not present before (Gray et al., 2018). The accretion of this section of the island contrasts sharply with the ~1.7 km stretch of Central Bird Shoal's shoreline, which eroded significantly from 2014 to 2018, retreating by a maximum of 70 m and losing a majority of its continuous dune ridge. This section, being the least protected by Bogue and Shackleford Banks and lying perpendicular to Beaufort Inlet, is likely particularly vulnerable to erosion (Seymour et al., 2019). Further morphological changes were observed at the eastern end of Bird Shoal, which exhibited spit growth into the channel of Deep Creek, growing eastward by ~250 m and expanding seaward by ~45 m between 2014 and 2018 (Seymour et al., 2019). Low dunes also emerged on this section of the island over the same period (Seymour et al., 2019). A habitat cover change analysis by Gray et al. (2018) revealed a significant increase in the amount of supratidal sand cover within the RCR between 2004 and 2017 related to the dramatic eastward lengthening of Bird Shoal.

Based on the findings of Seymour et al. (2019), Bird Shoal exhibited significant geomorphological changes, such as accretion, erosion, and post-storm recovery, outside of storm events between 2014 and 2018, deviating from the FLBI archetype proposed by Pilkey et al. (2009). The observed foreshore recovery, landward retreat, and overwash processes on Bird Shoal more closely resemble those documented on open-ocean barrier islands (Seymour et al., 2019). This study builds on the work of Seymour et al. (2019) and aims to evaluate ongoing geomorphological and land cover changes within the RCR, with a specific focus on Bird Shoal, over the past five years. Understanding the shifting dynamics of Bird Shoal and the RCR as a whole holds significance for several reasons. Firstly, monitoring changes to the geomorphology and habitats of the RCR advances our understanding of the Reserve's evolution and the coastal resilience that it provides for the town of

Beaufort. Secondly, by examining changes in the morphology of Bird Shoal, we validate Bird Shoal's departure from the FLBI model, addressing a gap in understanding of how inlet barrier islands respond to alterations to their inlet. Thirdly, shifts in land cover offer insights into succession patterns within the RCR and reveal how habitats are adapting to morphological changes. Ultimately, this comprehensive survey of the Reserve advances our understanding of inlet barrier island dynamics and provides valuable data for documenting continued changes to the RCR.

Methods

Data Collection Summary

The 2023 unoccupied aircraft system (UAS) aerial survey of the Rachel Carson Reserve consisted of six flight missions that took place over five separate days in March and April of 2023 (Figure 1, Table 1). The survey captured 8,032 georeferenced images of the RCR across the six flight missions. Flight missions overlapped slightly with adjacent missions to facilitate image calibration for the merged data products. The foundation of this survey builds upon previous work by Seymour et al. (2019), who also conducted UAS surveys of the RCR in May 2018, establishing a baseline for longitudinal studies.

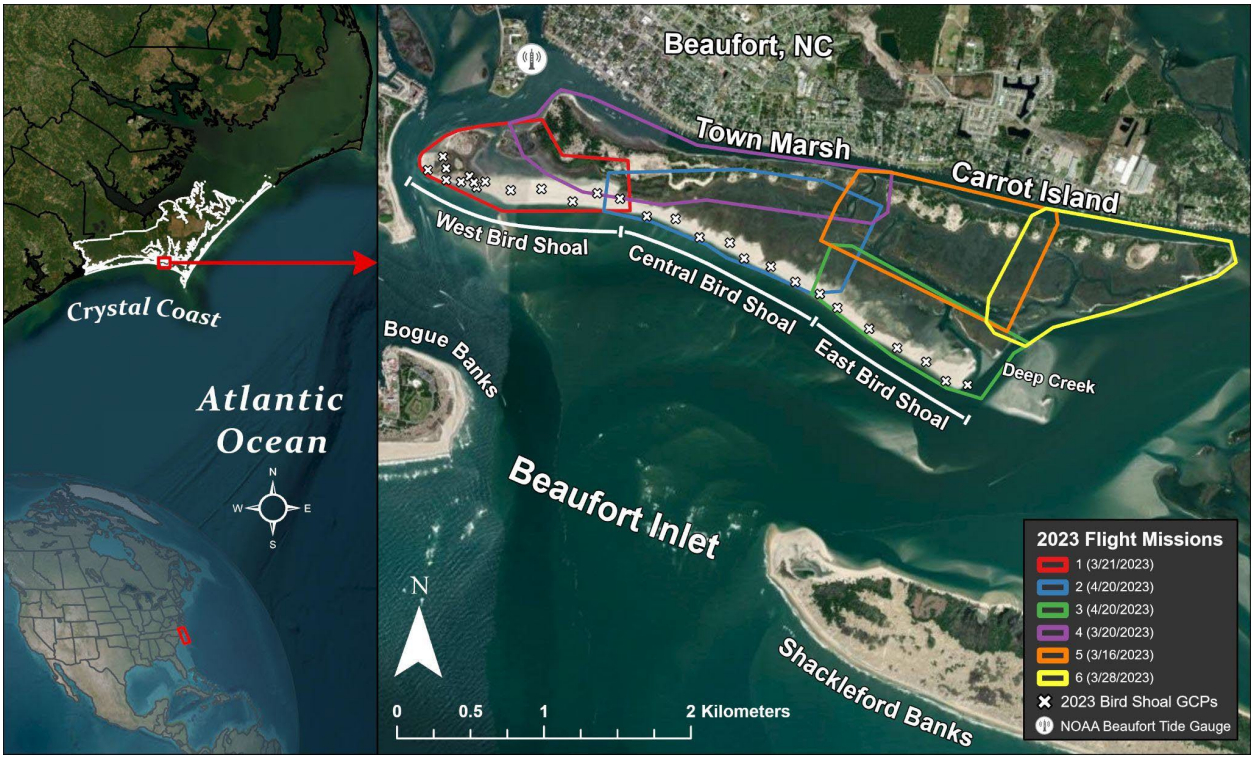

Figure 1: The Rachel Carson Reserve Study Area with 2023 flight mission coverage areas and ground control point locations. Base imagery of the RCR are the orthomosaics generated by each flight mission. All other base layer imagery is from the ArcGIS Pro basemap options with service layer credits to NC CGIA, Maxar, ESRI, TomTom, Garmin, FAO, NOAA, USGS, EPA, NPS, and USFWS.

Table 1: Metadata for each flight mission and the products generated from their imagery. Accuracy metrics were provided in Pix4D processing reports. For datasets that include GCPs, the accuracy metrics are based on the elevation model's variance from the GCPs. For datasets that do not include GCPs, accuracy metrics are based on position error of the eBee X's onboard GNSS receiver and adjusted for the computed image position in Pix4D. The Merged Bird Shoal mission was created by merging Missions 1-3 in Pix4D.

	Mission 1	**Mission 2**	**Mission 3**	**Mission 4**	**Mission 5**	**Mission 6**	**Merged Bird Shoal**
Date	3/21/2023	4/20/2023	4/20/2023	3/30/2023	3/16/2023	3/28/2023	3/21 - 4/20/2023
Location	West Bird Shoal	Center Bird Shoal	East Bird Shoal	Town Marsh	West Carrot Island	East Carrot Island	Bird Shoal
No. of Flights	2	3	2	3	1	3	7
Flight Coverage (km^2)	0.553	1.02	0.97	1.32	1.21	1.00	1.82
Avg GSD (m)	0.0249	0.0254	0.0247	0.0261	0.0262	0.0262	0.0248
GCPs	13	10	7	0	0	0	29
RMS error (X/Y/Z (m))	0.0114/ 0.0215/ 0.0181	0.0085/ 0.0140/ 0.0063	0.0563/ 0.0279/ 0.0115	0.0227/ 0.0210/ 0.0179	0.0204/ 0.0216/ 0.0209	0.0238/ 0.0259/ 0.0195	0.0337/ 0.0202/ 0.0151
Sigma (X/Y/Z (m))	0.0114/ 0.0215/ 0.0181	0.0085/ 0.0140/ 0.0063	0.0563/ 0.0279/ 0.0115	0.0227/ 0.0210/ 0.0179	0.0204/ 0.0216/ 0.0209	0.0238/ 0.0259/ 0.0195	0.0337/ 0.0202/ 0.0151
Mean (X/Y/Z (m))	0.0001/ -0.0001/ -0.0010	0.0000/ 0.0000/ 0.0000	0.0002/ -0.0001/ 0.0002	0.0002/ 0.0003/ 0.0000	0.0000/ 0.0001/ -0.0002	-0.0001/ -0.0000/ 0.0001	0.0001/ 0.0000/ -0.0004

UAS Platform and Sensors

Imagery for the 2023 survey was captured using a senseFly Duet T camera, equipped with an RGB sensor optimized for drone applications (S.O.D.A., 5472 x 3648 image format), which was attached to a senseFly eBee X fixed-wing unoccupied aircraft. The eBee X was outfitted with an onboard survey-grade GPS system, which allowed for the application of post-processing kinematic corrections using raw GNSS observations downloaded from the NOAA CORS (Continuously Operating Reference Station) in Beaufort, NC (NCBE) on flight days, improving the coordinate accuracy of geotagged images. Each flight was programmed for autonomous data collection at ~80 m above ground level using the eMotion3 flight management software (senseFly, Switzerland). Images were captured at 1-7° off nadir. Flight transects were spaced to achieve 75% lateral overlap and 80% longitudinal overlap between adjacent images. The chosen overlap ratings aimed to optimize the photogrammetric reconstruction process in regions of the RCR characterized by minimal color variation and texture, like near the water's edge for example. Flights were conducted at low tide during the morning or afternoon when the sun angle was low enough to minimize sun glint off the water in the imagery.

Ground Control Points

Before conducting the three flights over Bird Shoal, 29 square mats, each measuring 1.21 square meters and featuring an iron-cross pattern distinguishable from the sky, were evenly positioned across the island (Figure 1). These mats served as ground control points (GCPs) to improve georeference accuracy of the Bird Shoal datasets. The x, y, and z coordinates of the center of each GCP were measured with an Emlid Reach RS2+ survey-grade GPS system. GCP coordinate data was collected at intervals of 30 seconds, with the estimated RMS errors for the x, y, and z coordinates being less than 0.005 m. Unlike the Bird Shoal missions, missions 4, 5, and 6 covering Town Marsh and Carrot Island did not employ GCPs, as the precise mapping of geomorphological changes in these areas was not a priority for this study.

Orthomosaic and DSM Processing

Imagery from each mission was processed separately using Pix4D Mapper (Pix4D, Switzerland), a "Structure-from-Motion" (SfM) photogrammetry software, which generated orthomosaics and digital surface models (DSM) for each mission. We followed the Pix4D geoprocessing settings protocol presented by Puckett et al. (2022), which were optimized for coastal wetland mapping. GCPs were registered in Pix4D for flight missions that contained them to improve the georeference of the data products. Data products from each mission were referenced to the WGS 1984 UTM 18N horizontal projection and had ground sampling distances less than 0.03 meters. Missions that included GCPs were referenced to the NAVD88 (m) vertical datum while missions that did not include GCPs were referenced to height above the WGS 84 ellipsoid (m). Elevation data products referenced to height above the WGS 84 ellipsoid were not used for the purposes of the present study. Notably, the area coverage statistics from the GCP-referenced missions are smaller than the true flight coverage. This discrepancy is due to the removal of images from the intertidal area between Bird Shoal and the land-facing islands, a step taken to enhance rectification accuracy. After initial processing, the three GCP-referenced missions covering Bird Shoal were merged together in Pix4D, creating a continuous orthomosaic and DSM of the island.

Derived Data Products Analysis

To highlight the geomorphological transformations of the Rachel Carson and Bird Shoal in particular over the span of five years, we conducted various analyses using the orthomosaic and DSM products generated by the SfM process. Analyses were conducted in ArcGIS Pro 3.1 (ESRI Inc., Redlands, CA, USA) and ArcMap (ESRI Inc., Redlands, CA, USA).

Because the SfM process relies on optically and positionally consistent features in imagery to facilitate dataset construction, processing dynamic aquatic areas can result in visual and elevation artifacts over water surfaces in orthomosaics and DSMs respectively. To remove the inaccurate water surface artifacts from the processed datasets, the orthomosaics and DSMs were masked to the non-aquatic area of the RCR. The RCR land mask was manually drawn using the orthomosaics and DSMs as reference so as to remove any artifacts.

Contours

To visualize topographic and shoreline changes across Bird Shoal, two sets of contour lines were produced, one for 2023 and one for 2018. The 2023 contours were generated from the merged Bird Shoal DSM processed for this study. The 2018 contours were generated using a DSM of Bird Shoal

produced from the next most recent UAS survey of Bird Shoal flown on 5/22/2018 by Seymour et al. (2019). The 2018 survey contained 14 GCPs, which were measured using an Emlid Reach RS. The 2018 and 2023 DSMs were both referenced to NAVD88 meters for their vertical coordinate system, ensuring that elevation data were comparable across datasets. The 2018 DSM, originally processed in Pix4D, had a vertical RMS error of 0.042 m (additional accuracy metrics for the 2018 DSM can be found in Seymour et al. (2019)). The contour sets from 2018 and 2023 consisted of contour lines generated at 0.25 m intervals, ranging from -0.75 m to 8.75 m to capture geomorphological changes from intertidal areas to upland areas. Contour sets were then cleaned for DSM elevation artifacts by removing lines smaller than 10 m for contours of ≤ 0 m of elevation, and by removing lines smaller than 5 m for contours of ≥ 0 m of elevation. Then, the contour lines were smoothed to further reduce the effect of DSM elevation artifacts using the *Smooth Line* tool in ArcGIS Pro.

Shoreline Change

The Digital Shoreline Analysis System (DSAS; Himmelstoss et al., 2018), an ArcMap tool developed by the U.S. Geological Survey, was used to quantify shoreline change distances and rates. Shoreline contours of Bird Shoal were extracted from the 2018 and 2023 contour sets at the 0.50 m elevation contour. For reference, the mean higher high water (MHHW) tidal datum for Beaufort, North Carolina lies at 0.445 m, mean sea level (MSL) at -0.112, and mean lower low water (MLLW) at -0.633 m relative to NAVD88. Table 2 lists shoreline contours used in the shoreline change analysis and their respective accuracy measurements derived from the DSM SfM processing reports.

Table 2: List of contour lines used to define Bird Shoal's shorelines in the shoreline change analysis. The table also includes the estimated accuracy for each shoreline used in the DSAS analysis. Change measurements calculated by DSAS are only as certain as the accuracy associated with the shoreline contours they are derived from. Uncertainty for the 2023 shoreline is the combined horizontal and vertical RMS error associated with the Merged Bird Shoal Dataset. The uncertainty value associated with the 2018 shoreline was derived from accuracy statistics validated by Seymour et al. (2019) using elevation checkpoints. A horizontal accuracy assessment was not conducted for this dataset.

Collection Dates	Elevation Contour (m)	Sensor	Uncertainty (m)
03/21-04/20/2023	0.50	senseFly S.O.D.A.	0.069
05/22/2018	0.50	senseFly S.O.D.A.	0.042

The two vectorized contours of Bird Shoal's shoreline in 2018 and 2023 were combined into one layer for processing with DSAS. First, DSAS was used to cast cross-shore transects at 50 m intervals, generating a total of 75 transects across Bird Shoal's ocean-facing southern shoreline. To ensure that transects were consistently cast at a perpendicular angle to Bird Shoal's curved shoreline, an offshore baseline transect was vectorized parallel to the general shape of the shoreline transects. Another baseline was vectorized at the eastern end of Bird Shoal to cast alongshore transects to measure eastward growth of the island. A total of 14 transects were cast from this baseline at an interval of 10 m. Then, DSAS was used to calculate shoreline change statistics along each transect. Change statistics included Net Shoreline Movement (NSM), Shoreline Change Envelope (SCE), and End Point Rate (EPR). Finally, transects were clipped to the SCE for visualization purposes.

Elevation Change

To analyze elevation changes across Bird Shoal, we compared the 2023 DSM we generated to the 2018 DSM of Bird Shoal from Seymour et al. (2019). Each DSM was masked to the area above the

0.50 m elevation "shoreline" contour line and resampled to a 3 cm cell size to ensure a consistent spatial resolution. The 0.50 m contour line was chosen as it was the lowest possible elevation contour that did not include artifacts resulting from the SfM process and provided a continuous polygon to mask the area of Bird Shoal to in both time steps.

An elevation difference surface (EDS) was generated using a surface-subtraction equation (Eq. (1)) on the 2018 and 2023 DSMs. Because the two DSMs did not overlap in areas where Bird Shoal had changed dramatically, such as where land had eroded into the water between 2018 and 2023, elevation differences could not be calculated for these areas. To account for these areas, we delineated polygons around areas that experienced a complete gain or loss of land above the 0.50 m elevation contour between the years of 2018 and 2023 (Figure 6).

Eq. (1) $EDS = DEM_{2023} - DEM_{2018}$

Volumetric Change

A volumetric change analysis was conducted to quantify changes to the land volume of Bird Shoal. We used the EDS generated for the elevation change analysis to account for volumetric change where the 2018 and 2023 DSMs overlapped. To account for significant landform changes outside of where the datasets overlapped, two separate rasters were created using the land gained and lost polygons generated in the elevation change analysis. The 2023 DSM was masked to the land gained feature class to create an elevation surface for land entirely gained above the 0.50 m contour line between 2018 and 2023. The 2018 DSM was masked to the land lost feature class to create an elevation surface for land that was eroded below the 0.50 m elevation contour between the two time periods, like land that transitioned into water because of shoreline migration for example. This process resulted in three distinct rasters for volumetric analysis: the EDS, the DSM of land gained, and the DSM of land lost.

Elevation values in the EDS and the DSMs tracking land gained or lost that fell below the combined vertical RMS error of the contributing datasets were excluded and masked out from the analysis because these values were below the threshold for detection. For instance, for the EDS, the cumulative vertical RMS error of the two datasets used in the comparison was 0.0571 m, so any positive or negative values between -0.0571 and 0.0571 were considered as no elevation change. Only values outside of the respective vertical RMS errors of the 2018 and 2023 were considered for the land lost and land gained DSMs. Cells outside of this error range were used to compute the volume of sediment that had either accumulated or eroded between the two time periods.

The volumes of accreted and eroded sediment on Bird Shoal above the 0.50 m contour line were calculated using Eq. (2) and Eq. (3) where V is the volume of sediment (m^3), Z_{EDS} is the elevation value for each cell in the EDS, Z_{Gained} is the elevation value for each cell in the DSM of land gained, Z_{Lost} is the elevation value for each cell in the DSM of land lost, and $dxdy$ is the cell area (0.03 × 0.03 m^2). The accretion and erosion volume equations only account for positive and negative elevation change values in the Z_{EDS} respectively. Thus, the volumetric analysis of the EDS calculates volumetric change in areas where the 2018 and 2023 DSMs overlapped above the 0.50 m elevation contour, while the land gained and land lost DSMs offered insights into the total volume of sediment accreted or eroded in areas experiencing significant landform transitions above the 0.50 m contour.

Eq. (2): $V_{accretion} = \sum max(0, Z_{EDS})dxdy + \sum Z_{Gained}dxdy$

Eq. (3): $V_{erosion} = \sum min(0, Z_{EDS})dxdy - \sum Z_{Lost}dxdy$

Net sediment volume change above the 0.50 m elevation contour was calculated using Eq. (4) where ΔV_{net} is net volumetric change (m^3) on Bird Shoal from 2018 to 2023.

Eq. (4): $\Delta V_{net} = V_{accretion} - V_{erosion}$

To account for the volumetric change measurement error, we summed the cubic meters associated with the vertical RMS error for the datasets involved in the comparison. For instance, for EDS accretion measurements between 2018 and 2023 (167,651.5 m^2), our volume error measurement was 9,572.9 m^3 (4/20/2023 error of 0.0151 m^3 m^{-2} + 5/22/2018 error 0.042 m^3 m^{-2}).

Habitat Classification

The habitat classes used to classify the RCR were established based on the NERRS Habitat and Land Cover Classification Scheme (NERRSCS), designed to ensure consistency in classification methods for researchers working within the NERRS. This framework not only covers broad habitat categories such as wetland and upland but also includes more specific subclasses identified by the primary vegetation types found within each subclass. Table 4 provides details of the relevant NERRSCS classes used in this study. The NERRSCS framework has been used to map the habitats of the RCR since 2004, with the most recent classification having been conducted in 2017 by Gray et al. (2018), allowing for a habitat change analysis.

To conduct our habitat classification of the RCR, we follow a similar methodology to Gray et al. (2018), which used UAS imagery to inform the classification of the RCR in Worldview-3 and RapidEye satellite imagery. Because vegetation types and the transition zones between habitats are clearly visible in ultra-high resolution UAS imagery, UAS-derived orthomosaics can be effectively used as ground-truth data to assist in the generation of training data for habitat classifiers and to validate their results (Gray et al., 2018).

For this study, we elected to use imagery from the Sentinel-2 Earth observation satellite constellation because it is open-access and has a revisit rate of 10 days, meaning we could source satellite imagery close to the flight dates and tide state of the 2023 UAS RCR survey missions. We obtained a single Level 2 Sentinel-2 image of the RCR and the surrounding region captured on 4/15/2023 from the Copernicus Open Access Hub. The Sentinel-2 image was referenced to the WGS 84 UTM 18N projection, allowing for direct comparison with the UAS-derived orthomosaics from 2023. In ArcGIS Pro, a seven-band composite raster was created that included each of the four 10 m Sentinel-2 bands, one 20 m infrared band resampled to 10 m resolution, as well as a normalized difference vegetation index (NDVI) and a normalized difference water index (NDWI) generated from the 10 m bands, as suggested by Carle et al., 2014 (Table 3). The satellite image was masked to the RCR to improve processing time.

Habitat classification was conducted in ArcGIS Pro. Training areas were outlined manually by creating polygons for each habitat type using the UAS orthomosaic as a reference dataset (Figure 2). Accounting for the influence of the UAS data's geolocation accuracy on polygon digitization was not necessary given the resolution of the Sentinel-2 image. Training polygons contained ≥ 10,000 m^2 of each class to capture spectral variation (Table 2). A Support Vector Machine (SVM) integrated into the *Classify* tool in ArcGIS Pro was then used to classify the Sentinel-2 image, with the manually drawn training polygons serving as training data for the classification of each habitat.

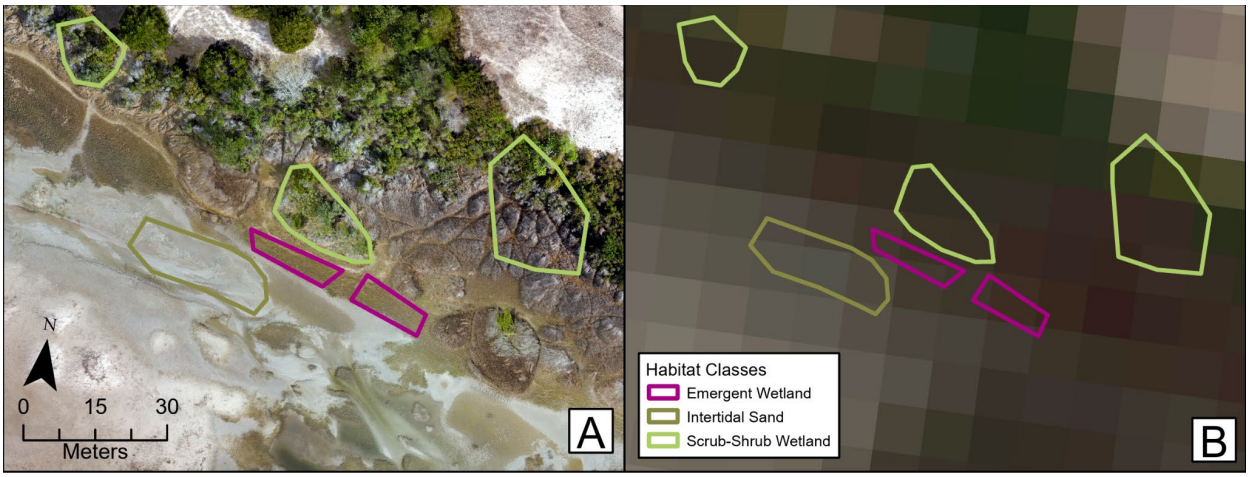

*Figure 2: (**A**) shows a UAS mosaic of the area between the islands of Bird Shoal and Town Marsh that was used as a reference to manually delineate habitat training polygons. A subset of the training polygons is visible as an example. (**B**) shows the Sentinel-2 image in true color of the same area and with the same training polygons. Note: the UAS imagery is 333 times higher resolution than the Sentinel-2 imagery, allowing for accurate habitat training class generation.*

Table 3: Bands included in the composite Sentinel-2 raster of the Rachel Carson Reserve. The Sentinel-2 image these bands were pulled from was captured on 4/15/2023 at 15:49:31 UTC.

Band	Resolution	Central Wavelength	Description
B2	10 m	490 nm	Blue
B3	10 m	560 nm	Green
B4	10 m	665 nm	Red
B8	10 m	842 nm	Visible and Near Infrared
WVP	10 m	945 nm	Water Vapor (Resampled from 20 m to 10 m)
NDVI	10 m	(B8-B4)/(B8+B4)	Normalized Difference Vegetation Index
NDWI	10 m	(B3 - B8) / (B3 + B8)	Normalized Difference Water Index

To determine the accuracy of the 2023 habitat classification map, we generated 198 randomly distributed points across the RCR using the *Create Accuracy Assessment Points* tool in ArcGIS Pro. The points were overlaid on the UAS orthomosaics, and the true habitat classes for each point were assessed using the UAS imagery. With the accuracy assessment points, we used the *Compute Confusion Matrix* tool to generate a confusion matrix. All visual validation was conducted by the same individual to ensure consistency.

To conduct the habitat change analysis, the classified habitat map of the RCR produced by Gray et al. (2018) via the classification of a WorldView-3 image captured on 8/31/2017 was obtained with permission from the authors (additional dataset metadata can be found in Gray et al. (2018)). To ensure consistent spatial resolution across timesteps, the 2017 habitat classification raster was resampled from a cell size of 1.2 m to a 10.0 m cell size to match the resolution of the 2023 Sentinel-2 habitat classification map produced for this study. Each habitat classification raster was converted to a polygon using the *Raster to Polygon* tool, which provided area statistics for each habitat class. The tide state at the time of the 2023 Sentinel-2 image acquisition was +0.23 m above

the Mean Lower Low Water (MLLW) tidal datum. For reference, the Worldview-3 image used by Gray et al. (2018) to conduct the 2017 habitat classification of the RCR was acquired during a tide state of +0.22 m above MLLW, so differences in tide state between the two datasets are negligible. Water level measurements were taken from the NOAA tidal reference station in Beaufort, North Carolina (CO-OPS Station ID: 8656483; 34°43.2'N, 76°40.2'W).

Table 4: The habitat classes and subsystems of the National Estuarine Research Reserve System Classification Scheme used to map the Rachel Carson Reserve. All habitat subsystems of the Rachel Carson Reserve are under the Estuarine system type. This table is adapted from Gray et al. (2018).

Class	ID	Subsystem	Definition
Subtidal Haline	2100	Subtidal Haline	the substrate is continuously submerged [by tidal water and] . . . ocean-derived salts measure [at least] 0.5h during the period of average annual low flow.
Intertidal Sand	2253	Intertidal Haline	unconsolidated particles smaller than stones [constitute at least 25% aerial cover and] are predominantly sand. Particle size ranges from 0.00625 mm to 2.0 mm in diameter.
Emergent Wetland	2260	Intertidal Haline	characterized by erect, rooted, herbaceous hydrophytes, excluding mosses and lichens. This vegetation is present for most of the growing season in most years. These wetlands are usually dominated by perennial plants
Supratidal Sand	2323	Supratidal Haline	unconsolidated particles smaller than stones [constitute at least 25% aerial cover and] are predominantly sand. Particle size ranges from 0.00625 mm to 2.0 mm in diameter.
Scrub-Shrub Wetland	2350	Supratidal Haline	includes areas dominated by woody vegetation less than 6 m (20 feet) tall. The species include true shrubs, young trees, and trees or shrubs that are small or stunted because of the environment.
Upland Sand	6123	Supratidal Upland	unconsolidated particles smaller than stones [constitute at least 25% aerial cover and] are predominantly sand. Particle size ranges from 0.00625 mm to 2.0 mm in diameter.
Herbaceous Upland	6131	Supratidal Upland	herbaceous upland habitat that is dominated by graminoids.
Scrub-Shrub Upland	6140	Supratidal Upland	includes areas dominated by woody vegetation less than 6 m (20 feet) tall. The species include true shrubs, young trees, and trees or shrubs that are small or stunted because of the environment.
Forested Upland	6150	Supratidal Upland	characterized by woody vegetation that is 6 m tall or taller. All water regimes are included except subtidal.

Subsystem	Definition
Intertidal Haline	the substrate is exposed and flooded by tides; includes the associated splash zone; . . . ocean-derived salts measure [at least] 0.5h during the period of average annual low flow
Supratidal Haline	nontidal wetlands containing at least 0.5h ocean- derived salts at some point during a year of average rainfall.
Supratidal Upland	any coastal upland area above the highest spring tide mark that is periodically over-washed, covered, or soaked with seawater during storm events to an extent that affects habitat structure or function.

Results

Shoreline Change

The two shoreline contours used in the shoreline change analysis for Bird Shoal are shown in Figure 3. Shoreline change measurements were taken by comparing the southern ocean-facing shorelines to one another. Between 2018 and 2023, the island's area increased by 8.9 hectares above the 0.50 m contour line, from 39.1 hectares in 2018 to 48.0 hectares in 2023.

Shoreline change statistics for each of the 75 cross shore transects provide information on how the position of Bird Shoal's shoreline shifted between 2018 and 2023 (Figure 5, Table 5). Transects can be broken into two types based on the shoreline change they recorded: erosional (shoreline dist. increased from the baseline) or accretional (shoreline dist. decreased from the baseline). Table 5 shows that the majority of transects experienced erosion between 2018 and 2023, showing that most of Bird Shoal's shoreline moved landward, closer to the town of Beaufort. Additionally, the magnitude of the mean erosion distance was higher than that of the mean accretion distance for transects that recorded each respective measurement. The greatest accretional NSM recorded was 62.54 m and was located on the ocean-facing lobe that developed on West Bird Shoal (Figure 4A). The greatest erosional NSM recorded was -80.16 m, which occurred at the eastern end of Bird Shoal where the end of the island retreated but also elongated (Figure 4D). Bird Shoal elongated by 292.7 m when comparing the difference between the island's easternmost extents in 2018 and 2023, as shown in Figure 4D. Figure 5 shows the EPR for each shoreline transect along the shoreline of Bird Shoal. There is clear spatial variation in the type and magnitude of shoreline change across the island. West Bird Shoal recorded both retreat along its escarpment and shoreline growth along the ocean-facing lobe. Transects along Central and East Bird Shoal all recorded landward shoreline movement, with retreat generally increasing moving east along the island.

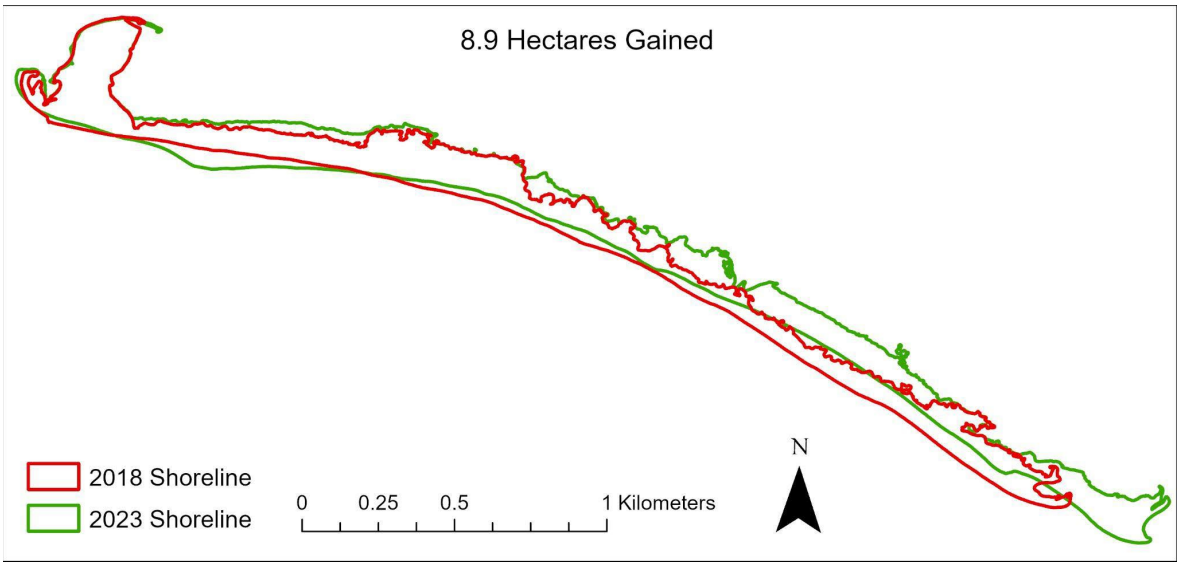

Figure 3: Shorelines of Bird Shoal from May 2018 and April 2023 derived from the 0.50 m elevation contour relative to NAVD88.

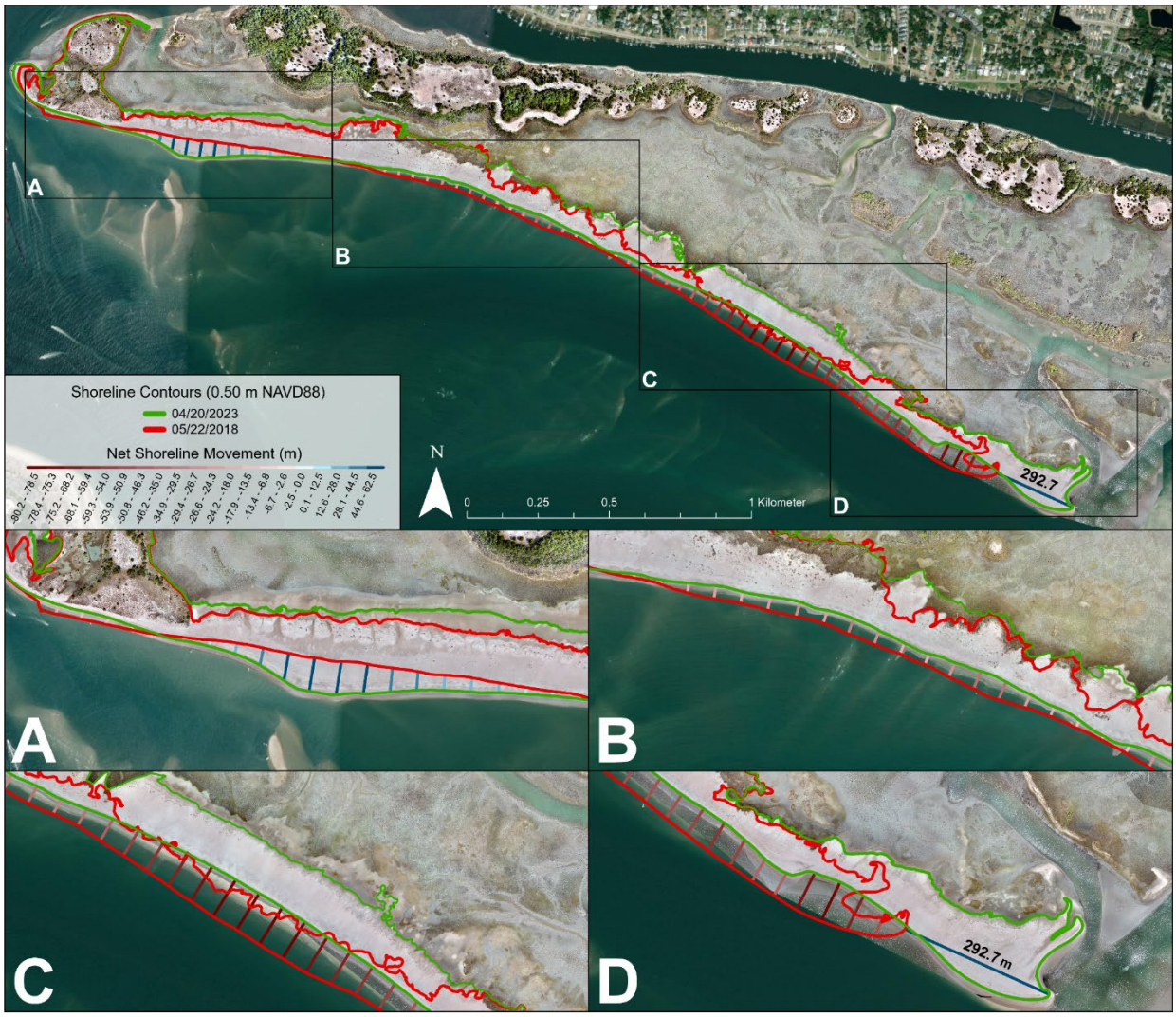

*Figure 4: Shoreline change transects symbolized by net shoreline movement values. (**D**) shows the net shoreline movement of the eastward-most extents of Bird Shoal between 2018 and 2023. It should be noted that EPR assumes a linear relationship for the amount of erosion per year, which is likely not the case between the two time steps.*

Table 5: Statistics generated by the shoreline change NSM and EPR models in DSAS for Bird Shoal's shoreline change between 2018 and 2023.

Percent of erosional transects		77.33%	Percent of accretionary transects		22.67%
Net Shoreline Movement (NSM; m)	NSM mean erosion	-38.79	End Point Rate (EPR; m/yr)	EPR mean erosion	-7.9
	NSM mean accretion	28.66		EPR mean accretion	5.83
	NSM max. erosion	-80.16		EPR max. erosion	-16.32
	NSM max. accretion	62.54		EPR max. accretion	12.73

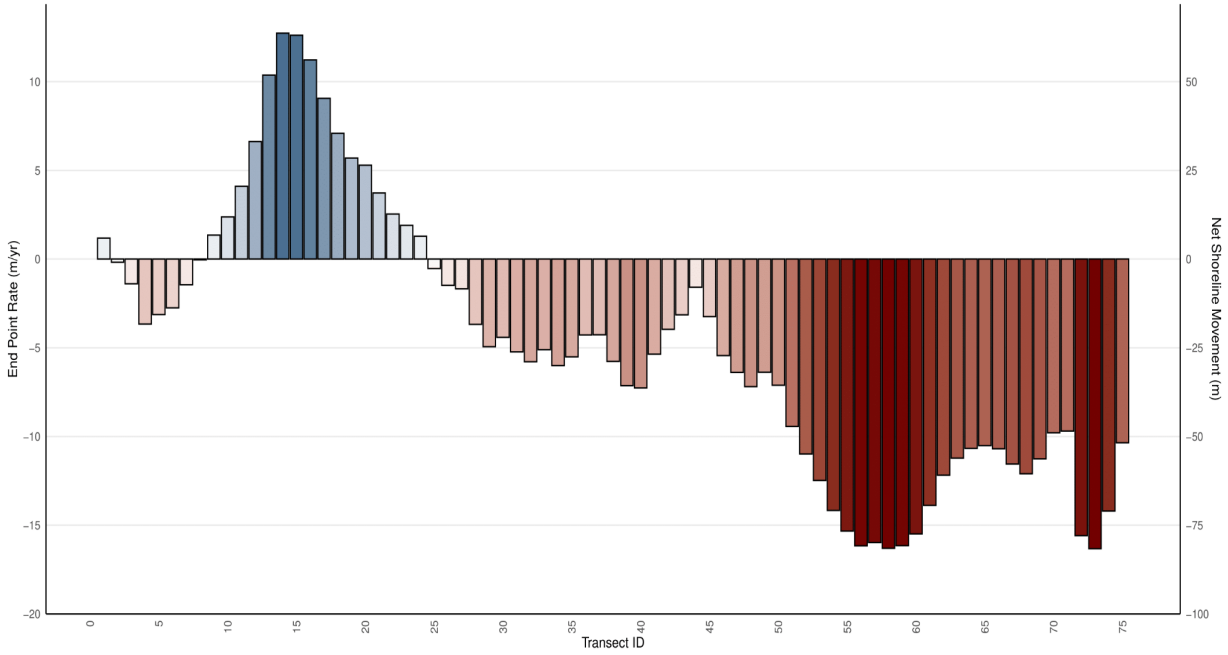

Figure 5: End point rate and net shoreline movement for shoreline transects across Bird Shoal. Transect ID increases traveling eastward along Bird Shoal's shoreline.

Elevation and Volumetric Change

Comparing the elevation products derived from the 2018 and 2023 DSMs demonstrates noticeable topographic changes across Bird Shoal. The elevation difference surface, along with DSMs clipped to where land was gained and lost above the 0.50 m elevation contour between 2018 and 2023 is shown in Figure 6. Accretion of sediment between 2018 and 2023 is represented by green areas while erosion is represented by red areas. From 2018 to 2023, areas of Bird Shoal lost 131,662.4 ± 6,828.5 m^3 of sediment and accreted 242,742.5 ± 12,529.7 m^3 of sediment, resulting in a net accretion of 111,080.1 ± 19,358.2 m^3. Patterns of erosion and accretion vary across the island.

Landward migration of Bird Shoal's shoreline, evidenced by overwash fans in the tidal flat, contributed to the majority of volumetric erosion recorded in the volumetric change analysis. Central and East Bird Shoal experienced the most shoreline erosion across the island (Figure 5). Central Bird Shoal experienced loss of shoreline to water above the 0.50 m elevation contour, as well as erosion on the extent of its 2023 forebeach area. East Bird Shoal experienced more significant shoreline migration, with this section of the island shifting completely past its landward extent in 2018. Therefore, the entire area of East Bird Shoal in 2018 contributed to the volume eroded between 2018 and 2023. Shoreline change shows the erosion of West Bird Shoal's escarpment, with elevation loss up to 3 meters, and lost land entirely in some areas above 0.50 m of elevation with respect to 2018 (Figure 6A). While elevation gains can be seen on the eastern end of the escarpment, there appears to be little inland deposition of sediment along the rest of the scarp. The 1.50 m elevation contours from 2018 and 2023 correspond with the front of the vegetated escarpment and demonstrate the significant erosion of this area, resulting in the separation of the escarpment from an adjacent dune that it was connected to in 2018, pictured in the bottom right panel of Figure 8. From 2018 to 2023, West Bird Shoal also experienced a loss in elevation and volume along the runnel behind the large ocean-facing lobe, as well as in many of the chutes between the hummocky dunes on this part of the island (Figure 6A).

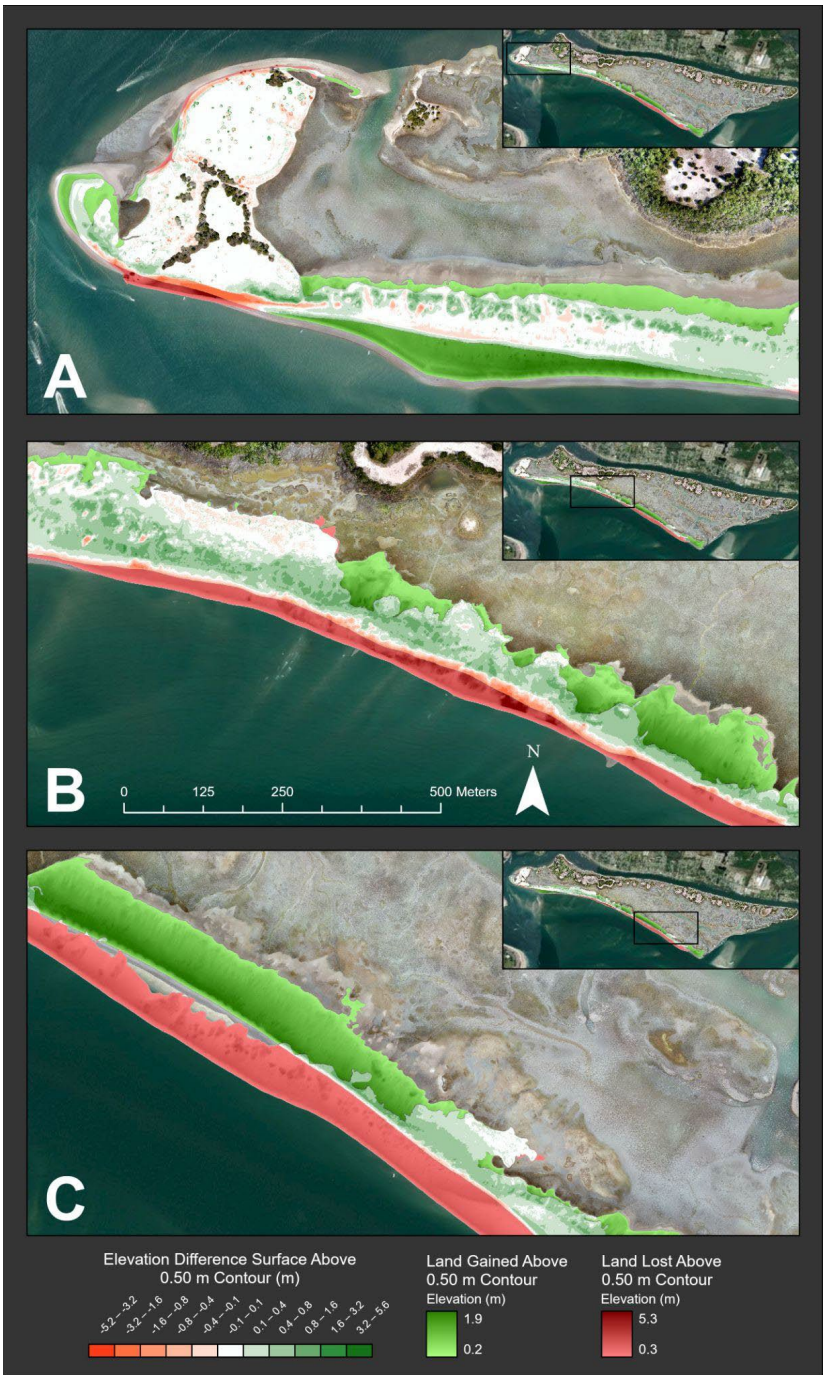

*Figure 8: Maps of the elevation difference surface between 2018 and 2023 for Bird Shoal. Polygons representing land gained (green) and lost (red) between 2018 and 2023 are overlaid on elevation models of the gained/lost land. (**A**) shows West Bird Shoal and (**B**) shows Central Bird Shoal. Service layer credits to NC CGIA, Maxar, and Earthstar Geographics.*

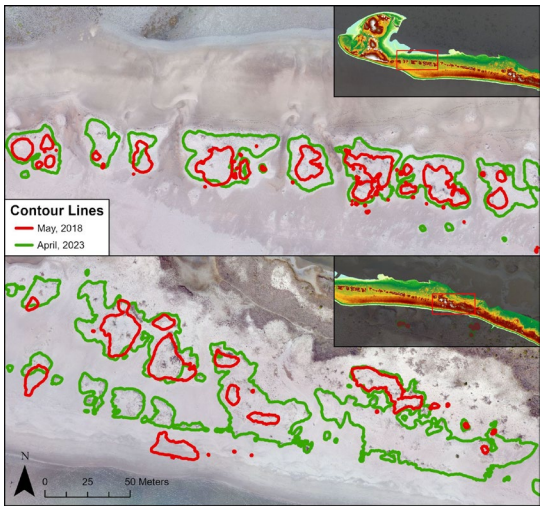

Figure 7: A visualization of dune growth on Bird Shoal. The top panel shows dune growth on West Bird Shoal, with dunes represented by the 1.25 m contour. The bottom panel shows dune growth on Central Bird Shoal, with dunes represented by the 1.75 m contour. A higher elevation contour line was chosen for Central Bird Shoal to help distinguish dune area from the overall higher elevation of the surrounding topography compared to West Bird Shoal. The map inset is a 2023 DSM of Bird Shoal to give topographic context. Base imagery is the 2023 orthomosaic of Bird Shoal generated by Pix4D.

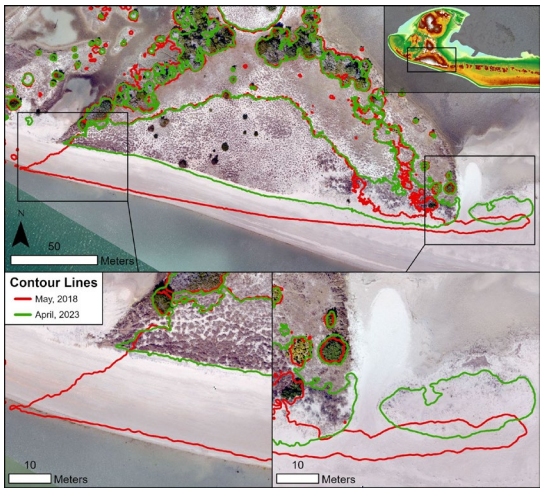

Figure 6: the 1.50 m contour overlaid on imagery of West Bird Shoal's beach, berm, and upland area. Service layer credits to NC CGIA, Maxar, and Microsoft. The map inset is a 2023 DSM of Bird Shoal to give topographic context. Base imagery is the 2023 orthomosaic of Bird Shoal generated by Pix4D.

Despite the recorded elevation and volume losses, Bird Shoal as a whole gained sediment volume. The development of overwash fans from storms contributed significantly to elevation and volume increases across the island. Because of the observed landward shoreline migration, Central and East Bird Shoal experienced inland deposition of overwash sediment extending into the intertidal area between Bird Shoal and Carrot Island (Figure 6B and 6C). Overwash processes appear to have increased land area above the 0.50 m elevation contour and widened the island in certain areas, resulting in overall volumetric accretion. The growth of dunes on Bird Shoal also contributed to these gains in elevation and volume. As illustrated in Figure 7, the dunes on the western side of Bird Shoal saw significant accretion, with some dune peaks on Central Bird Shoal increasing by up to 2 meters. The 1.25 and 1.75 m contour lines in Figure 7 highlight the footprints of discontinuous dunes on the western side of the island, which exhibited widening and increases in elevation between May 2018 and April 2023. Additionally, embryonic dune growth is evident in front of the main dune ridge along West and Central Bird Shoal. Furthermore, the expansion of the ocean-facing lobe (Figure 6A) and the eastward extension of the island (Figure 5D) also played a significant role in adding subaerial land above the 0.50 m elevation contour, enhancing the island's overall volume.

Table 6: Volumetric changes for Bird Shoal between 5/22/2018 and 4/20/2023. The total volume of Bird Shoal in 2023 is included for reference, measured using the DSM clipped to the area above the 0.50 m contour line.

Bird Shoal Total Volume in 2023 (m^3)	**Erosion (m^3)**	**Accretion (m^3)**	**Net Change (m^3)**
539,056.5	-131,662.4 ± 6,828.5	+242,742.5 ± 12,529.7	+111,080.1 ± 19,358.2

Habitat Change

A comparison of the resampled 2017 habitat classification map of the RCR produced by Gray et al. (2018) and the 2023 habitat classification produced for this study are shown side-by-side in Figure 9. Between 2017 and 2023, the upland sand and scrub-shrub upland habitats experienced the largest percent change, with upland sand decreasing by 44.4% and scrub-shrub upland increasing by 12.9%. Emergent wetland saw the largest increase in area gained, growing by 5.47 hectares. Much of this growth can be seen in the intertidal area between Central Bird Shoal and the northern islands (Figure 9). Herbaceous upland, which increased its area coverage by 8.6%, had much more of a presence at the center of Town Marsh in 2023 compared to 2017 (Figure 9). Additionally, the landward retreat of Bird Shoal is clear when comparing the increase in subtidal haline area on the southern extent of the habitat maps.

Figure 10 shows a flow diagram of habitat class transitions between 2017 and 2023, representing how much area has moved from one habitat class to another. The expansion of the emergent wetland habitat was largely due to the transition of intertidal sand into emergent wetland areas. However, intertidal sand habitats maintained a similar area coverage between 2017 and 2023. The supratidal sand, subtidal haline, and intertidal sand classes exchanged habitat coverage with one another, demonstrating the dynamic nature of Bird Shoal' shoreline. Similarly, the woody vegetation classes—scrub-shrub wetland, scrub-shrub upland, and forested upland—each exchanged area with one another from 2017 to 2023. The growth in herbaceous upland appears to be mainly drawn from exchange with the upland sand and scrub-shrub upland classes.

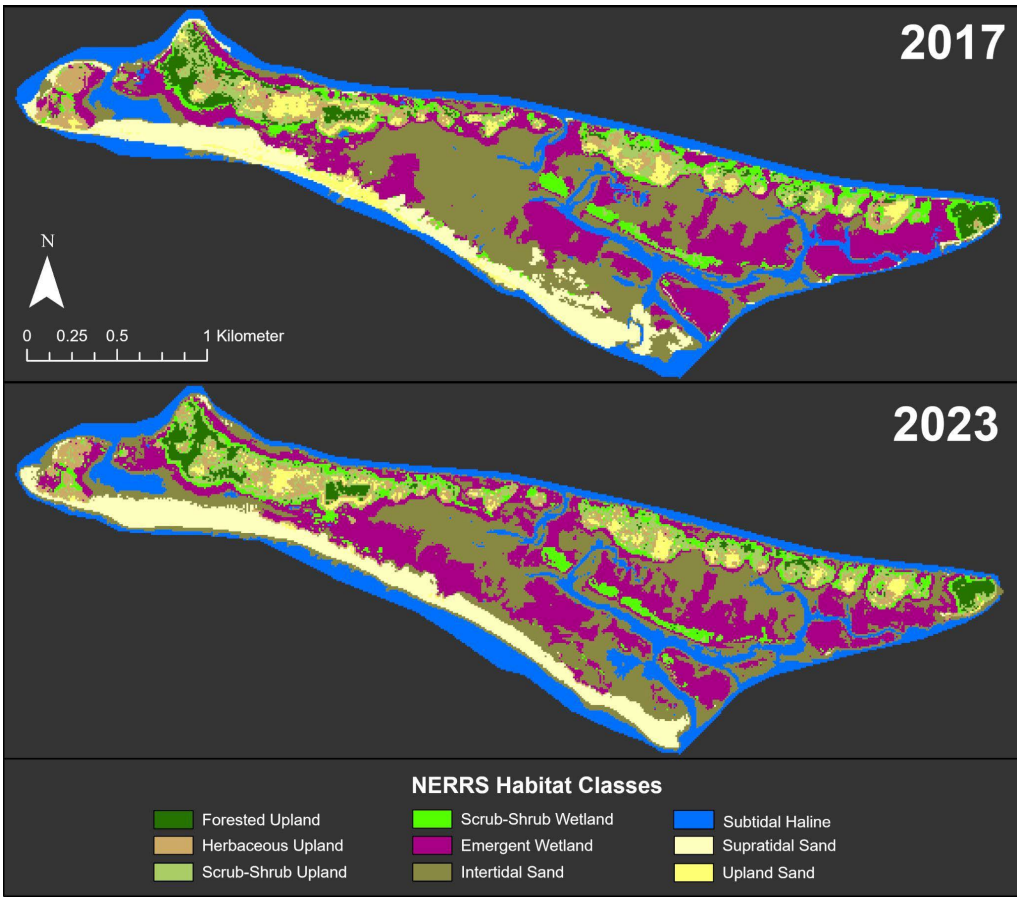

Figure 9: NERRS Habitat and Land Cover Classification Scheme maps of the Rachel Carson Reserve for 2017 and 2023. Both maps cover the same area. The 2017 map was derived from Gray et al. (2018).

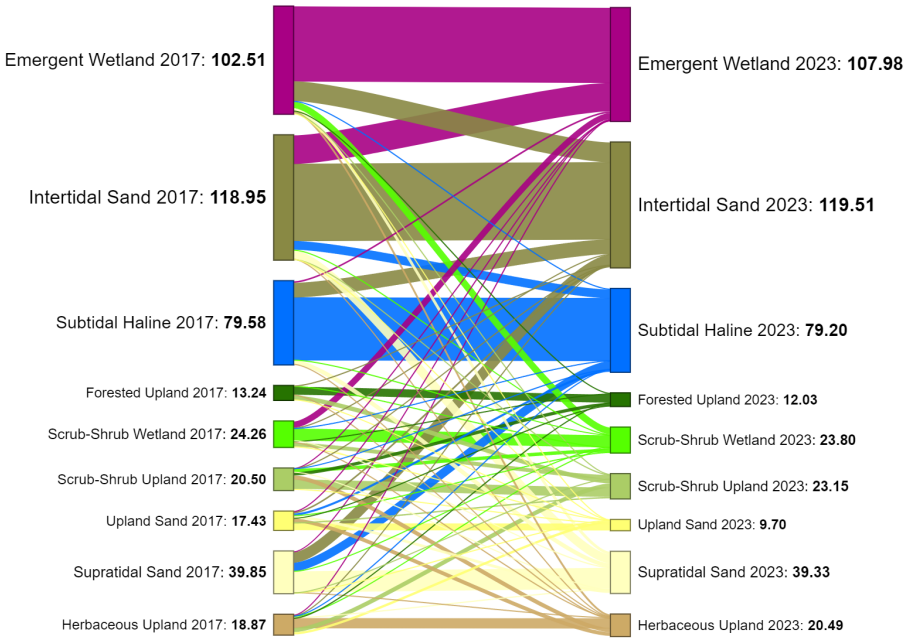

Figure 10: Area change in hectares for each habitat class from 2017 to 2023 based on the habitat classification maps (Fig. 9).

Accuracy for the 2023 Sentinel-2 habitat classification is shown in Table 7. The 2023 habitat classification of the RCR achieved an accuracy of 0.82 and a kappa statistic of 0.80. The confusion matrix in Table 7 shows the user and producer accuracies for each class. The intertidal sand, subtidal haline, supratidal sand, and forested upland classes each had high user and producer accuracies. The emergent wetland class was often confused with the scrub-shrub wetland class. Similarly, scrub-shrub wetland was confused with scrub-shrub upland. Upland sand also suffered from decreases in classification accuracy as a result of confusion with the herbaceous upland and scrub-shrub upland classes.

Table 7: Confusion matrix for the 2023 habitat classification map. Each cell holds a number of accuracy assessment points associated with each class. The columns describe UAS reference truthing and the rows describe the habitat class predicted by the classification process. Correctly classified habitats are on the major diagonal.

	Reference Class										
Habitat Class	**1**	**2**	**3**	**4**	**5**	**6**	**7**	**8**	**9**	**Total**	**User's Acc**
Emergent Wetland-1	**20**	2	0	0	0	0	0	0	0	22	91%
Intertidal Sand-2	0	**22**	0	0	0	0	0	0	0	22	100%
Subtidal Haline-3	0	0	**22**	0	0	0	0	0	0	22	100%
Scrub-Shrub Wetland-4	7	0	0	**13**	0	0	1	1	0	22	60%
Supratidal Sand-5	0	1	0	0	**21**	0	0	0	0	22	95%
Forested Upland-6	0	0	0	0	0	**22**	0	0	0	22	100%
Herbaceous Upland-7	2	0	0	0	0	0	**15**	3	2	22	68%
Scrub-Shrub Upland-8	1	0	0	1	0	3	6	**7**	4	22	32%
Upland Sand-9	0	0	0	0	1	0	0	0	**21**	22	95%
Total	30	25	22	14	22	25	22	11	27	198	82%
Producer's Accuracy	66%	88%	100%	93%	95%	88%	68%	64%	78%		

Discussion

This semi-decadal synoptic analysis comparing remotely-sensed datasets of the Rachel Carson Reserve from 2017/18 and 2023 recorded shoreline, elevation, and volumetric changes on Bird Shoal, as well as habitat changes across the entire Reserve. Morphodynamic changes across Bird Shoal, characterized by both accretion and erosion, indicate that the island represents a mixed energy system, confirming the hypothesis by Seymour et al. (2019) that Bird Shoal lacks conformance with the FLBI model put forth by Pilkey et al. (2009). The results of the present study

appear to demonstrate that morphological changes on Bird Shoal may be connected to the wave dynamic changes caused by widening of the Beaufort Inlet. Furthermore, habitats within the RCR may be reacting to the observed geomorphological changes. These findings provide an example of how inlet barrier islands react to changes to their inlet, furthering our understanding of inlet barrier island evolution. Additionally, the results have implications for the management of the Rachel Carson Reserve within the NERRS.

Morphological Change

The extensive retreat of Bird Shoal's shoreline, as revealed by the shoreline change analysis, indicates that storms and persistent oceanic wave energy may have affected the morphology of the island during the study period. The majority of shoreline retreat was concentrated on the eastern side of the island, demonstrating an alongshore gradient in shoreline erosion rate and landward migration (Figure 5). The gradient in shoreline migration across Bird Shoal contributed to a noticeable straightening of the island's shoreline relative to the orientation of Beaufort Inlet between 2018 and 2023. The presence of overwash fans stretching into the intertidal flat indicates that storm surges likely impacted Bird Shoal during the study period. However, given the finding of Seymour et al. (2019) that Bird Shoal exhibited recovery from storms, shoreline change may not be exclusively attributed to storm events. The heightened shoreline retreat observed on the eastern side of Bird Shoal may be attributed to diminished protection from oceanic wave energy, a consequence of significant erosion to Shackleford Banks located directly to the south of this section of Bird Shoal. Furthermore, the predominant wind climate and short fetch distances (≤ 4 km) around Bird Shoal suggest that shoreline changes, aside from the effects of storms, were driven by oceanic wave energy. These findings indicate that Bird Shoal might not conform to the FLBI model presented in Pilkey et al. (2009), which typically predicts limited morphological change in such short fetch conditions.

Along with the pronounced shoreline migration on the eastern side of Bird Shoal, the island also experienced considerable erosion on the vegetated escarpment of West Bird Shoal. From 2018 to 2023, the escarpment receded landward by up to ~20 meters, and experienced a loss of elevation of ~1.5-3 meters along the former seaward extent of the face. In the aftermath of Hurricane Matthew, Seymour et al. (2019) documented that this section of West Bird Shoal's shoreline was the only area exhibiting a trend of continuous erosion both before and after storm recovery. This trend looks to have continued from 2018 to 2023. Because of the lack of inland sediment deposition (Figure 6A), the escarpment's ~3 m elevation likely prevented it from being overtopped by storm surge waves during the study period, indicating that this part of the island conforms to the level 2 "collision regime" on the Sallenger Storm Impact Scale (Sallenger, 2000). Based on the Sallenger (2000) model, wave runup likely collides with West Bird Shoal's escarpment and transports sediment in the offshore or longshore direction, limiting the potential for overwash and subsequent sediment deposition on areas landward of the escarpment, contributing to continuous erosion. However, there is evidence that the eastern end of the escarpment is undergoing natural stabilization, as indicated by the observed increase in elevation in this area landward of the receded scarp face since 2018 (Figure 6A).

Just east of the escarpment, many of the chutes between the discontinuous dunes on West Bird Shoal also experienced erosion. Similarly, the runnel fronting the dune ridge behind the ocean-facing lobe on West Bird Shoal decreased in elevation over the study period. The lack of accretion in these areas is likely a result of more persistent overwash or tidal flooding from the back barrier embayment (e.g., Figure 6A, which shows flooding of the chutes and runnel on West Bird Shoal following Hurricane Ian in 2022). The runnel and dune chutes, which range between 0.5 m and 1.0 m of elevation, are likely interconnected and flood together when high tides or storm surges increase water levels above MHHW (0.445 m).

Figure 11: UAS aerial imagery of West Bird Shoal captured before and after Hurricane Ian passed by the Crystal Coast in October, 2022.

Despite the observed shoreline retreat and erosion of the island, the comparison of Bird Shoal's shorelines in 2018 and 2023, as depicted in Figure 3, demonstrates an overall increase in land area. This signals a net accretionary trend over the five-year period, supported by the volumetric change analysis. Overwash processes significantly contributed to the expansion of Bird Shoal's area by facilitating the migration of the island. During the study period, the RCR experienced three hurricanes (Florence (2018), Dorian (2019), and Ian (2022)), along with several tropical and north eastern storms, with each event causing water levels to surpass the Mean Higher High Water (MHHW) mark as recorded by a tidal gauge located approximately 1 km from the study area (Figure 1; National Ocean Service station BFTN7, Beaufort, NC). The impact of storms are evidenced by overwash deposits on the tidal flat of Bird Shoal (Figure 6) that originated from water levels overtopping dunes on the island, indicating that storm events which occurred during the study period reached at least a level 3 “overwash regime” on the Sallenger Storm Impact Scale (Sallenger, 2000). Visual inspection of Figure 4 and Figure 6 shows that on sections of Central and East Bird Shoal where shoreline change transects recorded erosion, the corresponding backbarrier side of the island exhibited land gain or accretion as a result of overwash. In some cases, overwash deposits resulted in the widening of the island above the 0.50 m elevation contour which compensated for land lost to shoreline migration (Figure 6B, 6C). Similar to the observations on Bird Shoal, open ocean-facing barrier islands commonly widen as overwash processes naturally extend tidal flats and push dunes landward (e.g. Riggs and Ames, 2007; Deaton et al., 2017). The pattern of island widening through overwash processes is what allows barrier islands to migrate landward and maintain resilience to storms and rising sea levels (Donlan and Godfrey 1973;

Penland et al., 1985; Walters and Kirwan 2016; Zinnert et al., 2019). Considering that Bird Shoal exhibited a net increase in sediment volume between 2018 and 2023, it appears that overwash processes effectively retained sediment within the system, compensating for volumetric decreases above the 0.50 m elevation contour as a result of shoreline migration. Storm activity may have also indirectly contributed to sediment deposition on Bird Shoal through the net import of sediment into the sound and deposition of sediment on flood tidal deltas near Bird Shoal (FitzGerald et al., 2002; Castagno et al., 2018; Georgiou et al., 2024).

In addition to the increased sediment distribution facilitated by storms and overwash processes, sediment may also have been redistributed to the tidal flat or captured by dunes via aeolian transport during the study period. This process likely contributed to the observed increases in the elevation and volume of sediment in these areas (Figure 6A), which was documented on Bird Shoal following a storm by Seymour et al. (2019). The increased height and width of dunes on West and Central Bird Shoal suggest effective trapping and stabilization of aeolian-transported sediment by dune vegetation (Feagin et al., 2015), which has become more prevalent on the dune field of Bird Shoal since 2018 (personal unpublished observation). The dune accretion observed between 2018 and 2023 indicates that the dunes on West and Central Bird Shoal have recovered from previous storms and did not undergo significant or persistent overwash just prior to the 2023 survey, as such events typically result in the flattening of dunes (Sallenger, 2000; Miller et al., 2010; Gornish and Miller, 2010).

Cross shore sediment transport may have played a significant role in the growth of the ocean-facing lobe on the shoreline of West Bird Shoal, contributing to the overall increase in the area and volume of the island. According to Seymour et al. (2019), “Western Bird Shoal became contiguous with a flood delta shoal” in 2010, as migrating shoals filled an alongshore ebb channel that formerly separated the delta from the shoreline. The welding of this migratory shoal to the shoreline resulted in substantial accretion and the growth of an ocean-facing lobe. Tidal currents and oceanic waves drive the movement of flood tidal deltas within estuaries; ocean swells can push these deltas inland via cross-shore transport, while ebb channel flows can counteract or reverse this movement (Austin et al., 2018). It is likely that direct exposure to ocean wave energy from Beaufort Inlet facilitated the cross shore transport that led to the landward migration and welding of flood tidal delta shoals to the shoreline, thereby increasing the area and volume of West Bird Shoal. Similar dynamics of swash bars migrating onshore through wave energy have been observed at mixed-energy inlets, such as Essex River Inlet and Parker River Inlet (Smith and FitzGerald, 1994; Hine, 1975). This process indicates that Bird Shoal is influenced by oceanic wave energy, particularly during high tide when water levels over the flood tidal delta shoals increase, rather than being solely controlled by limited fetch dynamics typical of FLBI systems (Pilkey et al., 2009; Smith et al., 2010).

Like the dynamics of cross-shore sediment transport, bidirectional alongshore transport from Central Bird Shoal may have similarly resulted in increases to island volume and land area by contributing to lobe growth and lateral spit growth on the eastern end of Bird Shoal (Seymour et al., 2019). Alongshore currents likely encountered the intertidal shoals near the eastern extremity of Bird Shoal in 2018, depositing entrained sediment on the shoals. This sediment deposition would have likely increased the shoals' elevation, making them subaerial and contiguous with the island, thereby contributing to the lengthening and volumetric accretion of Bird Shoal. A similar process of island lengthening through longshore transport was observed and modeled by Hoan et al. (2011) for a barrier island in Sweden. Although barrier island elongation through spit growth is a common occurrence for ocean-facing barrier islands, these cases can be associated with the migration of a tidal inlet, which is not the case for Bird Shoal's elongation (Park and Wells, 2007; Hoan et al.,

2011). Nevertheless, sufficient wave energy is required to drive longshore transport (Komar and Inman, 1970; Stutz and Pilkey, 2011), indicating that Bird Shoal may be regularly exposed to oceanic wave energy penetrating Beaufort Inlet. Bird Shoal's persistent eastward growth, along with the the lobe growth on the western side of the island, suggests that both alongshore and cross shore transport are the primary drivers of change on Bird Shoal under prevailing conditions. These modes of sediment transport would not play as significant a role in shaping the morphology of the island if it were in a low-energy, fetch-limited system (Jackson et al., 2002), further indicating a departure from the typical conditions observed in such systems.

Building upon the observations of geomorphological changes and sediment dynamics on Bird Shoal, we introduce a conceptual model that further elucidates how modified wave dynamics, following the eastward expansion of Beaufort Inlet, may have influenced the evolution of Bird Shoal. This model specifically addresses how the altered geometry of Beaufort Inlet has reshaped the spatial distribution of wave energy, impacting the coastal morphology as detailed below. Between 1994 and 2010, minimal changes in the width of Beaufort Inlet maintained a consistent wave spread arc for ocean waves that penetrated the inlet and diffracted radially towards Bird Shoal. At the eastern and western extremities of Bird Shoal, wave influence on the shoreline was negligible because of protection by the ocean-facing barriers of Bogue and Shackleford Banks from waves approaching the inlet from the south. Therefore, net wave-driven alongshore sediment flux along the Bird Shoal shoreline approached zero at both ends. A zero-flux boundary condition, combined with the radial pattern of waves passing through the inlet, tends to produce a concave island shoreline shape, roughly analogous to the shape of a shoreline protected at each end by rocky headlands (Shih and Komar, 1994; Turki et al., 2013; Ratliff and Murray, 2014), with the island's cuspate shape tending to closely mirror the radial spread of the wave arc. These dynamics maintained Bird Shoal's length at approximately 3 km, focusing sediment dynamics within these limits rather than allowing for widespread redistribution of sediment beyond the island's longitudinal subaerial extents, such as onto the intertidal shoals facing Carrot Island on Bird Shoal's eastern side.

Following the significant erosion of Shackleford Banks starting around 2010 and the resultant eastward expansion of Beaufort Inlet, increased wave energy was able to penetrate the inlet. This asymmetric expansion shifted the wave spread arc predominately eastward, disrupting the previously established zero-flux boundary condition for alongshore transport at Bird Shoal and extending the boundary eastward. This shift facilitated increased sediment deposition along the intertidal shoals to the east of the island, leading these areas to become subaerial features integrated with the main body of Bird Shoal. Moreover, as the wave arc broadened eastward, Bird Shoal began adapting to the new, wider arc shape. This transformation led to the island's eastward widening towards the new zero-flux boundary, which resulted in the 292.7 m eastward elongation of the island, and a movement towards a straighter shoreline configuration. This straightening effect is most pronounced on Central and East Bird Shoal, where shoreline retreat adjusted to match the reduced angle of the diffracted wave arc, illustrating the dynamic response to the widening of Beaufort Inlet.

Habitat Change

Land cover changes across the RCR from 2017 to 2023 may be tied to the changing morphology of Bird Shoal, successional processes, and sea level rise. Examination of the interchange between the areas of the subtidal haline, intertidal sand, and supratidal sand classes demonstrate the shifts in sediment distribution around Bird Shoal during the study period also recorded by the shoreline and elevation change analyses. Because of the landward migration of Bird Shoal, areas of intertidal and supratidal sand transitioned into the subtidal haline class. Conversely, the growth of West Bird

Shoal's lobe and the end of East Bird Shoal converted subtidal haline area into intertidal and supratidal sand.

The impact of storm-induced overwash is apparent in the 2023 habitat map (Figure 9) through the formation of overwash fans, prominently observed on Central Bird Shoal as distinct deposits of supratidal sand extending into the tidal flat. Overwash and aeolian transport of sand from Bird Shoal into the landward tidal flat may have increased the elevation sufficiently to provide suitable habitat for the growth of salt marsh vegetation (Godfrey and Godfrey, 1974; Rodriguez et al., 2013). This process is evident in the low relief areas between Bird Shoal and the landward islands as substantial increases in emergent wetland transitioning from intertidal sand. Similarly, areas of exposed supratidal sand in the tidal flat of East Bird Shoal in 2017 have been converted to emergent wetland in 2023. Further salt marsh development is also seen near the tidal creek separating Town Marsh from Bird Shoal. The increase in emergent wetland may increase the resilience of Bird Shoal because backbarrier marshes, particularly those located in the tidal flat, work to stabilize barrier islands by reducing the backbarrier tidal prism and acting as a platform for sediment as the island migrates (FitzGerald et al., 2008, 2018; Walters et al., 2014; Lorenzo-Trueba and Mariotti, 2017). Additionally, these marshes enhance the resilience of the barrier islands to sea-level rise by conserving sand and protecting against storm breaching (Cañizares and Irish, 2008; Nienhuis et al., 2021). Increases to the area of emergent wetland may also provide additional habitat for avian and aquatic species, improve the availability of grazing areas for the Reserve's feral horse population, and increase the uptake of carbon within the Reserve (Pennings and Bruno and Bertness, 2001; Fear, 2008; Shepard et al., 2011).

Despite the overall growth of emergent wetland habitat across the RCR, the migration of Bird Shoal has led to sediment deposition covering salt marsh areas along the banks of the embayment between Town Marsh and Bird Shoal, causing emergent wetland to transition into intertidal sand in this area. However, loss of salt marsh in this area, and in other areas of the RCR, may also be tied to increased water levels as a result of sea level rise, which causes salt marsh die off through inundation and marsh bank erosion in intertidal areas (Morris et al., 2002; Fagherazzi et al., 2006; Kirwan and Megonigal, 2013). Gray et al. (2018) indicate the possibility for salt marsh recovery with a lower rate of sea level rise, but the low suspended sediment content in the area poses a barrier to marsh accretion, indicating that continuous sea level rise may hinder long-term recovery efforts.

Woody vegetation habitats (scrub-shrub wetland, scrub-shrub upland, and forested upland) increased in area coverage by approximately 2 hectares across the RCR from 2017 to 2023. The overall increase in woody vegetation suggests enhanced morphological stability within the ecosystem, as noted by Zinnert et al. (2016), with root systems aiding in sediment stabilization and erosion resistance. While extensive woody vegetation can enhance resilience by absorbing disturbance, it may also impede sediment transfer over longer timeframes, leading to significant shoreline erosion (Zinnert et al., 2016). Given that woody vegetation in the RCR exists primarily on Town Marsh and Carrot Island, which are protected from strong erosional forces by Bird Shoal, this negative resilience impact is not likely to impact the Reserve in the near future. An exception to this is the die off of maritime forest on the eastern end of Carrot Island caused by erosion of the shoreline from vessel wakes. This shift towards woody vegetation could potentially make the islands more susceptible to sea-level rise and salt-water intrusion, given the sensitivity of woody plants to salinity (Zinnert et al., 2016). With increased woody plant cover, there is a potential moderation of temperatures, as suggested by Thompson et al. (2017), which could alleviate extreme temperature stress on wildlife, particularly during summer months. This state change towards woody-dominated communities alters habitat quality for both birds and mammals, as

observed in Virginia barrier islands (Zinnert et al., 2016). Increased prevalence of mammalian predators, like red foxes and raccoons, in islands where woody habitats are increasing, threatens ground-nesting shorebirds, such as the piping plover (*Charadrius melodus*) and shrub-dependent birds (Erwin et al., 2001; Zinnert et al., 2016). In addition to the documented increase in woody vegetation, the habitat change comparison also revealed increases in graminoid vegetation cover in areas that were formerly bare upland sand on the high elevation points on Town Marsh, as shown by the transition from the upland sand habitat class to the herbaceous upland habitat class (Figure 10). This increase in grassland vegetation cover is likely to enhance the capacity of this section of Town Marsh to capture aeolian sediments. Contrary to the observed pattern of succession from grassland to woody vegetation on other North Atlantic barrier islands, as documented by Young et al. (2007) and Zinnert et al. (2016), such a transition does not appear to be occurring presently in the RCR.

Implications for the Future and Management of the Rachel Carson Reserve

The morphological and habitat changes to the Rachel Carson Reserve observed in this study offer insights into the Reserve's future evolution and help to shape informed management strategies. Morphological changes to the Beaufort Inlet and Bird Shoal are likely due in part to sea level rise, which continues to accelerate because of climate change (Khojasteh et al., 2023). Sea level rise has been intensified by interactions between the North Atlantic Oscillation and the El Niño Southern Oscillation, which have caused local sea level hotspots in the region since 2011 (Valle-Levinson et al., 2017). Higher water levels may cause further widening of the Beaufort Inlet (Portos-Amill et al., 2023) and accelerated sediment erosion or accretion of the RCR's shorelines, contingent on prevailing forcing patterns (Rodriguez et al., 2008; Theuerkauf et al., 2014). Erosion driven by sea level rise anomalies may also be increasing the susceptibility of Bird Shoal to overwash (Theuerkauf et al., 2014), which has also increased in frequency for ocean-facing barrier islands in North Carolina due to storms (White and Wang, 2003). Likewise, the relatively low elevation dunes along Bird Shoal and the disturbance-reinforcing vegetation that inhabit them make the island vulnerable to future overwash events and resulting shoreline migration (Zinnert et al., 2017). With future sea level rise, the landward migration of sections of Bird Shoal is likely to continue, which may result in the island moving further into the intertidal area of the RCR and closer to Town Marsh and Carrot Island. The rate of island migration will be controlled by future storm events, storm recovery, ongoing dynamics at Beaufort Inlet, and the pace of local sea level rise.

The observed increases in dune width and elevation on Bird Shoal suggest an enhanced capacity for these dunes to trap sediment entrained through aeolian transport, which is likely to promote future dune growth (Luna et al., 2011; Jackson and Nordstrom, 2011). This growth could strengthen Bird Shoal's role as a protective barrier for the adjacent islands and the town of Beaufort, safeguarding them from coastal hazards. However, the hummocky nature of the dunes continue to make Bird Shoal susceptible to overwash through the dune chutes, which perpetuates hummockiness (Goldstein et al., 2017). Because of the landward embayment, its narrow dunes, and the presence of dune chutes, West Bird Shoal may be vulnerable to breaching along its dune ridge in the event of extreme storm surge (Nienhuis et al., 2021). However, sediment supplied by shoal welding and alongshore transport would likely be sufficient to fill the breach, preventing its permanence (Robinson and McBride, 2003). Central Bird Shoal may present another area of potential vulnerability because diffracted waves may be focused towards its relatively narrow beach. A possible management strategy to reduce vulnerability to storms involves planting horizontally-growing dune vegetation in the chutes between the dunes on Bird Shoal, which may work to anneal the dunes and create a continuous dune ridge (Goldstein et al., 2017). Future efforts to monitor morphological changes are essential to document the rate of erosion and accretion on Bird Shoal,

especially if the Beaufort Inlet continues to widen. These observations can add context to inlet barrier island evolution and further the responsible management of the Rachel Carson Reserve.

The land cover observations presented in this study provide information on which areas of the Reserve are shifting in habitat type. Changes to the spatial distribution and area coverage of habitat types could affect the management of different ecosystems within the RCR. The evolution and succession of habitats may have direct and indirect implications for the Reserve's species diversity, which will need to be managed carefully in the future. For instance, the transformation of habitat types at the edges of different ecosystems may intensify edge effects, leading to interactions between distinct biological communities. These edge effects can alter ecological balances, affecting species composition and behavior (Kozakiewicz, 1993; Andrén, 1995; Wilson et al., 2007). Management strategies will need to adapt to these changing conditions, and continued monitoring of habitats can help to efficiently plan for such changes within the RCR.

Caveats

A major limitation of this study is its synoptic approach, which limits our analysis to generalizations of geomorphological forcings rather than assessing the effects of specific events like storms. For instance, we attribute accretion on the shoreface of West Bird Shoal (Figure 6A) to the landward migration of offshore flood tidal shoals based on the findings of Seymour et al. (2019). But without bathymetry data or imagery from before and after a storm to show flood tidal shoal movement towards the shore, the origin of the accreted sediment is uncertain. More frequent surveys would have enabled us to link specific observed geomorphological changes directly to individual events or wave conditions, thereby offering a more nuanced understanding of the factors driving change on the Rachel Carson Reserve.

While GCP-corrected DSMs produced by structure-from-motion have been found to have centimeter-level accuracy in barrier island environments (Seymour et al., 2018), ground-truthed elevation data would have provided a more ideal benchmark for measuring DSM error, ensuring even more precise and reliable assessments of elevation and volumetric changes on Bird Shoal. Ideally, we would have collected hundreds of RTK-GNSS data checkpoints across the entire Rachel Carson Reserve on the flight mission dates that measured latitude, longitude, elevation, and NERRSCS habitat type, which would have allowed for more comprehensive and precise accuracy assessments of our elevation, volumetric, and habitat change analyses.

It is important to note that our volumetric change assessment overestimates the volume of land accreted and eroded because it strictly focuses on volumetric changes above the 0.5 m elevation threshold. Masking the DSMs to the 0.50 m contour means that this analysis did not fully capture land volume changes at portions of the shoreface and backbarrier sections of the island. For instance, an area of Bird Shoal that eroded below the 0.50 m contour from 2018 to 2023 but remained above the water line would still be considered as land completely lost to the sea in this analysis. Similarly, an area of Bird Shoal above the water line but below the 0.50 m contour line in 2018 that experienced accretion, pushing it above the 0.50 m contour in 2023, would be categorized as newly gained land from 0.0 m, even though the transition represents a continuation of land already present, albeit at a lower elevation than 0.50 m. Consequently, by focusing exclusively on changes above the 0.50 m contour, the analysis overlooks the dynamics of erosion and accretion occurring just below this threshold, leading to an overestimate of volumetric changes on the shoreface. This constraint necessitates a cautious interpretation of the volumetric change findings, especially in the context of the dynamic nature of the RCR.

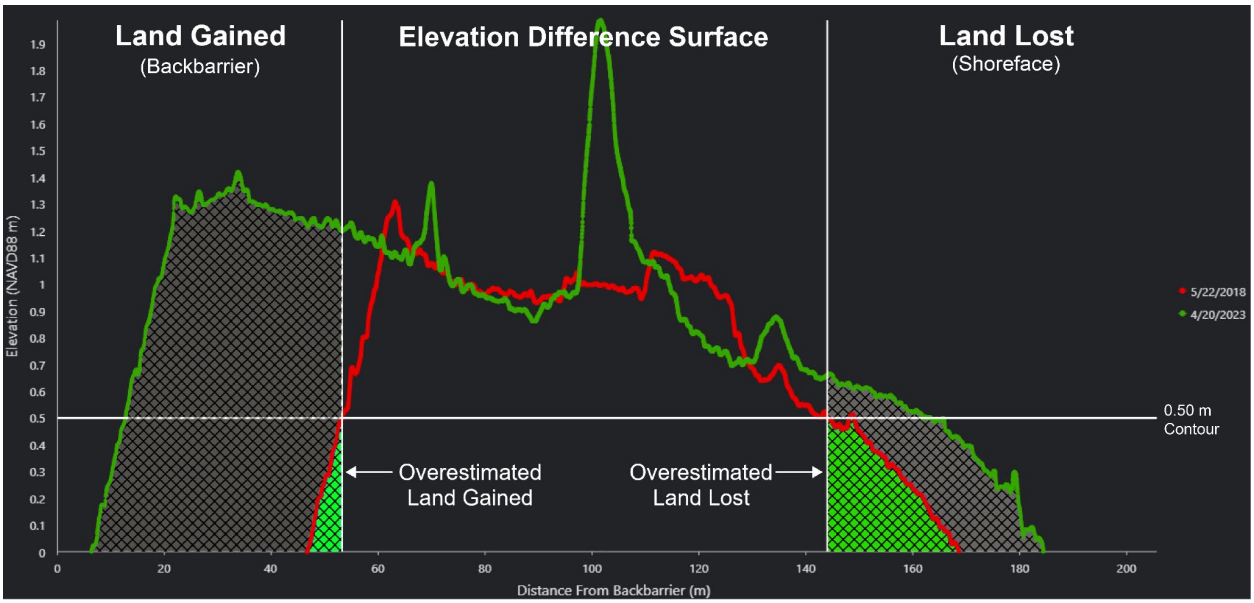

Figure 12: A visualization of the volumetric change assessment overestimation limitation. Elevation profiles taken from a transect of the 2023 and 2018 Bird Shoal DSMs show that the datasets do not overlap in areas of major change above the 0.5 m contour between timesteps (outside of vertical guidelines). The hatched areas represent the volume of land gained and land lost DSMs. Green hatched areas represent the accretion/erosion volume overestimation that arises as a result of this methodology.

While our habitat classification methodology was similar to Gray et al. (2018) in that we used UAS imagery to assist in the vectorization of NERRSCS training data to classify a satellite image of the RCR, there are notable differences in our approach. Unlike the 2017 study, which utilized high-resolution Worldview 3 imagery (0.3 m resolution), this study employed Sentinel-2 imagery, which offers a coarser resolution of 10 m. Consequently, our habitat map exhibits a coarser resolution, necessitating the resampling of the 2017 habitat map to align it with the current study's spatial scale. It is important to note that we did not conduct an accuracy assessment for the resampled 2017 map. Resampling is generally expected to degrade classification accuracy due to the loss of detail. In terms of image pre-processing, unlike Gray et al., who segmented their Worldview 3 imagery, we did not perform segmentation or radiometric calibrations on our Sentinel 2 image. The Sentinel-2 image used in the 2023 habitat classification was atmospherically corrected prior to acquisition, while no atmospheric corrections were applied to the Worldview-3 image. Additionally, the satellite imagery for the 2017 habitat classification map was captured in October while the 2023 habitat map was created using an image from April. This temporal difference likely resulted in spectral variations in vegetative cover due to seasonal changes that were not accounted for in our analysis. Future remote sensing studies of estuarine habitat change may choose to obtain higher-resolution satellite imagery with expanded spectral coverage, captured during the same season as older datasets, to enhance the accuracy of habitat classification products.

Our habitat classification methodology also differed slightly from Gray et al. (2018) because of the qualities of the remote sensing data used to generate the 2023 habitat classification map of the RCR, which may have influenced the accuracy and comparability of our habitat classification results. The spectral bands used in our Sentinel-2 composite raster image differed from those employed in the Worldview 3 composite used by Gray et al. (2018). While their Worldview 3 composite raster included a homogeneity texture filter layer and the standard coastal blue, yellow, red edge, and panchromatic bands, our Sentinel composite did not include these but did incorporate a Normalized Difference Water Index (NDWI) (reference recommending this?). Furthermore, we did

not remove water habitats from our classification using a spectral filter; instead, we classified the subtidal haline class using its own training dataset during supervised classification. For our SVM classification, elevation data was not used as a distinguishing factor between upland and wetland classes, whereas Gray et al. (2018) used the 0.9 m elevation contour to separate wetland from upland within their classification based on the NERRSCS class definitions. We did not pursue this step because of inconsistent elevation reference across the DSM datasets. This limitation arose because the Bird Shoal DSM datasets were registered to Ground Control Points (GCPs) referenced to NAVD88, while elevation data of the DSM datasets covering the rest of the Reserve were referenced to height above the WGS84 ellipsoid. This omission may have led to decreased class accuracy overall. For example, there was a notable reduction in the upland sand habitat classification for 2023. In the 2017 map, some areas of Central Bird Shoal's dunes were correctly classified as upland sand due to their elevation above 0.9 m, whereas in our 2023 map, no upland sand habitat was recorded in the same areas of Central Bird Shoal, reflecting these methodological limitations. Future studies employing the habitat classification methodology in Gray et al. (2018) should place and measure GCPs around their entire study area to maintain consistent elevation reference across elevation models.

Class confusion as demonstrated in the confusion matrix (Table 7) may have affected the interpretation of habitat class changes. For example, Figure 10 shows potential confusion between the emergent wetland and scrub-shrub wetland classes, as well as between the forested upland and scrub-shrub upland classes because these habitats exchanged area coverage with one another in the RCR from 2017 to 2023. This confusion may have arisen from the close proximity of these habitats to one another or from the mixing of vegetation types at habitat transition zones. Class confusion between the Upland Sand habitat and the Herbaceous Upland and Scrub-Shrub Upland habitats may have occurred because areas of upland sand, like on Town Marsh for example, can be interspersed with grasses and woody vegetation, complicating the identification of a clear dominant habitat class. This limitation, combined with mixing of estuarine habitats in close proximity to one another, may warrant a more “fuzzy” classification approach to improve accuracy for future habitat classification mapping using a similar methodology (Gray et al., 2018).

Acknowledgements

I am grateful for the support of many who have made this research possible. First, I would like to extend my gratitude to my advisor, Dr. Dave Johnston, whose guidance and mentorship have been invaluable throughout my time at Duke University. I am also thankful to Dr. Brad Murray for his expertise in framing the morphological processes critical to this study.

Special thanks go to MaRRS Lab members, Dr. Rett Newton and Josh Matheson, whose skillful piloting was essential for the success of our research. I also appreciate the staff of the North Carolina National Estuarine Research Reserve System for their cooperation and support.

On a personal note, I owe much to my parents for inspiring me to pursue my dreams, and to my partner, Hana Mamnoon, for her support and companionship throughout this research journey. Additionally, I am fortunate to have had the encouragement of my friends, who have been an incredible support system during both the highs and lows of this research process.

Each of you has played a pivotal role in this project, so thanks to all once more.

References

Anderson, C. P., Carter, G. A., & Funderburk, W. R. (2016). The Use of Aerial RGB Imagery and LIDAR in Comparing Ecological Habitats and Geomorphic Features on a Natural versus Man-Made Barrier Island. *Remote Sensing*, *8*(7), Article 7. https://doi.org/10.3390/rs8070602

Andrén, H. (1995). Effects of landscape composition on predation rates at habitat edges. In L. Hansson, L. Fahrig, & G. Merriam (Eds.), *Mosaic Landscapes and Ecological Processes* (pp. 225–255). Springer Netherlands. https://doi.org/10.1007/978-94-011-0717-4_10

Arkema, K. K., Guannel, G., Verutes, G., Wood, S. A., Guerry, A., Ruckelshaus, M., Kareiva, P., Lacayo, M., & Silver, J. M. (2013). Coastal habitats shield people and property from sea-level rise and storms. *Nature Climate Change*, *3*(10), 913–918. https://doi.org/10.1038/nclimate1944

Asbury H. Sallenger, Jr. (2000). Storm Impact Scale for Barrier Islands. *Journal of Coastal Research*, *16*(3), 890–895.

Austin, T. P., Vila-Concejo, A., Short, A. D., & Ranasinghe, R. (2018). A Multi-Scale Conceptual Model of Flood-Tide Delta Morphodynamics in Micro-Tidal Estuaries. *Geosciences*, *8*(9), Article 9. https://doi.org/10.3390/geosciences8090324

Barbier, E. B., Koch, E. W., Silliman, B. R., Hacker, S. D., Wolanski, E., Primavera, J., Granek, E. F., Polasky, S., Aswani, S., Cramer, L. A., Stoms, D. M., Kennedy, C. J., Bael, D., Kappel, C. V., Perillo, G. M. E., & Reed, D. J. (2008). Coastal Ecosystem-Based Management with Nonlinear Ecological Functions and Values. *Science*, *319*(5861), 321–323. https://doi.org/10.1126/science.1150349

Baustian, J. J., & Mendelssohn, I. A. (2015). Hurricane-Induced Sedimentation Improves Marsh Resilience and Vegetation Vigor under High Rates of Relative Sea Level Rise. *Wetlands*, *35*(4), 795–802. https://doi.org/10.1007/s13157-015-0670-2

Bruno, J., & Bertness, M. (2001). Habitat modification and facilitation in benthic marine communities. In *Marine Community Ecology* (Vol. 413, pp. 201–218).

Burns, J. M. (2015). Speciation in an Insular Sand Dune Habitat: Atrytonopsis (Hesperiidae: Hesperiinae)—Mainly from the Southwestern United States and Mexico—Off the North Carolina Coast. *The Journal of the Lepidopterists' Society*, *69*(4), 275–292.

Cañizares, R., & Irish, J. L. (2008). Simulation of storm-induced barrier island morphodynamics and flooding. *Coastal Engineering*, *55*(12), 1089–1101. https://doi.org/10.1016/j.coastaleng.2008.04.006

Carle, M. V., Wang, L., & Sasser, C. E. (2014). Mapping freshwater marsh species distributions using WorldView-2 high-resolution multispectral satellite imagery. *International Journal of Remote Sensing*, *35*(13), 4698–4716. https://doi.org/10.1080/01431161.2014.919685

Castagno, K. A., Jiménez-Robles, A. M., Donnelly, J. P., Wiberg, P. L., Fenster, M. S., & Fagherazzi, S. (2018). Intense storms increase the stability of tidal bays. *Geophysical Research Letters*, *45*(11), 5491–5500.

Castro-Bolinaga, C., Stark, N., Hall, S., & Massey, G. (2022). *Effects of Oyster Reefs on the Composition and Erodibility of Surrounding Bed Sediment*.

Crawford, T. (2007). North Carolina's Final Coastal Frontier: Land Cover Change in the Inner Banks, 1996-2001. *North Carolina Geographer*, *15*, 37–52.

Deaton, C. D., Hein, C. J., & Kirwan, M. L. (2017). Barrier island migration dominates ecogeomorphic feedbacks and drives salt marsh loss along the Virginia Atlantic Coast, USA. *Geology*, *45*(2), 123–126. https://doi.org/10.1130/G38459.1

DiGiacomo, A. E., Harrison, W. E., Johnston, D. W., & Ridge, J. T. (2020). Elasmobranch use of nearshore estuarine habitats responds to fine-scale, intra-seasonal environmental variation: Observing coastal shark density in a temperate estuary utilizing unoccupied aircraft systems (UAS). *Drones*, *4*(4), 74.

Dolan, R., & Godfrey, P. (1973). Effects of Hurricane Ginger on the Barrier Islands of North Carolina. *Geological Society of America Bulletin*, *84*(4), 1329. https://doi.org/10.1130/0016-7606(1973)84<1329:EOHGOT>2.0.CO;2

Erwin, R. M., Truitt, B. R., & Jiménez, J. E. (2001). Ground-Nesting Waterbirds and Mammalian Carnivores in the Virginia Barrier Island Region: Running out of Options. *Journal of Coastal Research*, *17*(2), 292–296.

Evans, J. (1988). Plant Succession and Stabilization of Dredge Spoil Habitats in the Rachel Carson National Estuarine Research Reserve; NC. *National Oceanic and Atmospheric Administration Technical Memorandum: Washington, DC, USA*.

Fagherazzi, S., Carniello, L., D'Alpaos, L., & Defina, A. (2006). Critical bifurcation of shallow microtidal landforms in tidal flats and salt marshes. *Proceedings of the National Academy of Sciences*, *103*(22), 8337–8341. https://doi.org/10.1073/pnas.0508379103

Feagin, R. A., Smith, W. K., Psuty, N. P., Young, D. R., Martínez, M. L., Carter, G. A., Lucas, K. L., Gibeaut, J. C., Gemma, J. N., & Koske, R. E. (2010). Barrier Islands: Coupling Anthropogenic Stability with Ecological Sustainability. *Journal of Coastal Research*, *26*(6), 987–992. https://doi.org/10.2112/09-1185.1

Fear, J. (2008). A Comprehensive Site Profile for the North Carolina National Estuarine Research Reserve.

FitzGerald, D., Buynevich, I., Davis Jr, R., & Fenster, M. (2002). New England tidal inlets with special reference to riverine-associated inlet systems. *Geomorphology*, *48*(1–3), 179–208.

FitzGerald, D. M., Fenster, M. S., Argow, B. A., & Buynevich, I. V. (2008). Coastal Impacts Due to Sea-Level Rise. *Annual Review of Earth and Planetary Sciences*, *36*(Volume 36, 2008), 601–647. https://doi.org/10.1146/annurev.earth.35.031306.140139

FitzGerald, D. M., J. Hein, C., Hughes, Z., Kulp, M., Georgiou, I., & Miner, M. (2018). Runaway Barrier Island Transgression Concept: Global Case Studies. In L. J. Moore & A. B. Murray (Eds.), *Barrier Dynamics and Response to Changing Climate* (pp. 3–56). https://doi.org/10.1007/978-3-319-68086-6_1

Fritz, H. M., Blount, C., Sokoloski, R., Singleton, J., Fuggle, A., McAdoo, B. G., Moore, A., Grass, C., & Tate, B. (2007). Hurricane Katrina storm surge distribution and field observations on the Mississippi Barrier Islands. *Estuarine, Coastal and Shelf Science*, *74*(1), 12–20. https://doi.org/10.1016/j.ecss.2007.03.015

Gedan, K. B., Altieri, A. H., & Bertness, M. D. (2011). Uncertain future of New England salt marshes. *Marine Ecology Progress Series*, *434*, 229–237.

Georgiou, I. Y., FitzGerald, D. M., & Hanegan, K. C. (2024). Storm and tidal interactions control sediment exchange in mixed-energy coastal systems. *PNAS Nexus*. https://doi.org/10.1093/pnasnexus/pgae042

Godfrey, P. J., & Godfrey, M. M. (1974). The role of overwash and inlet dynamics in the formation of salt marshes on North Carolina barrier islands. *Ecology of Halophytes*, 407–427.

Goldstein, E. B., Moore, L. J., & Durán Vinent, O. (2017). *Vegetation controls on maximum coastal foredune hummockiness and annealing time*. *Earth Surface Dynamics*. https://doi.org/10.5194/esurf-2017-2

Gornish, E. S., & Miller, T. E. (2010). Effects of storm frequency on dune vegetation. *Global Change Biology*, *16*(10), 2668–2675.

Gray, P. C., Ridge, J. T., Poulin, S. K., Seymour, A. C., Schwantes, A. M., Swenson, J. J., & Johnston, D. W. (2018). Integrating Drone Imagery into High Resolution Satellite Remote Sensing Assessments of Estuarine Environments. *Remote Sensing*, *10*(8), Article 8. https://doi.org/10.3390/rs10081257

Hay, M., & Wells, J. (1988). *Effects of feral horses on the production, distribution, abundance, and stability of salt marsh plants: Rachel Carson component of the National Estuarine Research Reserve.* (Final Report for NOAA Grant NA87AA-D-CZ023). North Carolina Department of Environment and Natural Resources.

Hayes, M. O. (1975). Morphology of Sand Accumulation in Estuaries: An Introduction to the Symposium. In L. E. Cronin (Ed.), *Geology and Engineering* (pp. 3–22). Academic Press. https://doi.org/10.1016/B978-0-12-197502-9.50006-X

Himmelstoss, E. A., Henderson, R. E., Kratzmann, M. G., & Farris, A. S. (2018). *Digital Shoreline Analysis System (DSAS) Version 5.0 User Guide*.

Hine, A. C. (1975). Bedford Distribution and Migration Patterns on Tidal Deltas in the Chatham Harbor Estuary, Cape Cod, Massachusetts. In L. E. Cronin (Ed.), *Geology and Engineering* (pp. 235–252). https://doi.org/10.1016/B978-0-12-197502-9.50019-8

Hoan, L. X., Hanson, H., Larson, M., & Kato, S. (2011). A mathematical model of spit growth and barrier elongation: Application to Fire Island Inlet (USA) and Badreveln Spit (Sweden). *Estuarine, Coastal and Shelf Science*, *93*(4), 468–477. https://doi.org/10.1016/j.ecss.2011.05.033

Houser, C., Wernette, P., Rentschlar, E., Jones, H., Hammond, B., & Trimble, S. (2015). Post-storm beach and dune recovery: Implications for barrier island resilience. *Geomorphology*, *234*, 54–63. https://doi.org/10.1016/j.geomorph.2014.12.044

Jackson, N. L., & Nordstrom, K. F. (2011). Aeolian sediment transport and landforms in managed coastal systems: A review. *Aeolian Research*, *3*(2), 181–196.

Jackson, N., Nordstrom, K., Eliot, I., & Masselink, G. (2002). "Low energy" sandy beaches in marine and estuarine environments: A review. *Geomorphology*, *48*, 147–162. https://doi.org/10.1016/S0169-555X(02)00179-4

Khojasteh, D., Haghani, M., Nicholls, R. J., Moftakhari, H., Sadat-Noori, M., Mach, K. J., Fagherazzi, S., Vafeidis, A. T., Barbier, E., Shamsipour, A., & Glamore, W. (2023). The evolving landscape of sea-level rise science from 1990 to 2021. *Communications Earth & Environment*, *4*(1), 1–11. https://doi.org/10.1038/s43247-023-00920-4

Kirwan, M. L., & Megonigal, J. P. (2013). Tidal wetland stability in the face of human impacts and sea-level rise. *Nature*, *504*(7478), 53–60. https://doi.org/10.1038/nature12856

Komar, P. D., & Inman, D. L. (1970). Longshore sand transport on beaches. *Journal of Geophysical Research (1896-1977)*, *75*(30), 5914–5927. https://doi.org/10.1029/JC075i030p05914

Kozakiewicz, M. (1993). Habitat isolation and ecological barriers—The effect on small mammal populations and communities. *Acta Theriologica*, *38*(1), 1–30. https://doi.org/10.4098/AT.arch.93-1

Lorenzo-Trueba, J., & Mariotti, G. (2017). Chasing boundaries and cascade effects in a coupled barrier-marsh-lagoon system. *Geomorphology*, *290*, 153–163. https://doi.org/10.1016/j.geomorph.2017.04.019

Luna, M. C. de M., Parteli, E. J., Durán, O., & Herrmann, H. J. (2011). Model for the genesis of coastal dune fields with vegetation. *Geomorphology*, *129*(3–4), 215–224.

Mariotti, G., & Hein, C. (2022). Lag in response of coastal barrier-island retreat to sea-level rise. *Nature Geoscience*, *15*, 1–6. https://doi.org/10.1038/s41561-022-00980-9

Miller, T. E., Gornish, E. S., & Buckley, H. L. (2010). Climate and coastal dune vegetation: Disturbance, recovery, and succession. *Plant Ecology*, *206*, 97–104.

Morris, J. T., Sundareshwar, P. V., Nietch, C. T., Kjerfve, B., & Cahoon, D. R. (2002). Responses of Coastal Wetlands to Rising Sea Level. *Ecology*, *83*(10), 2869–2877. https://doi.org/10.1890/0012-9658(2002)083[2869:ROCWTR]2.0.CO;2

Neumann, B., Vafeidis, A. T., Zimmermann, J., & Nicholls, R. J. (2015). Future Coastal Population Growth and Exposure to Sea-Level Rise and Coastal Flooding—A Global Assessment. *PLOS ONE*, *10*(3), e0118571. https://doi.org/10.1371/journal.pone.0118571

Nienhuis, J. H., Heijkers, L. G. H., & Ruessink, G. (2021). Barrier Breaching Versus Overwash Deposition: Predicting the Morphologic Impact of Storms on Coastal Barriers. *Journal of Geophysical Research: Earth Surface*, *126*(6), e2021JF006066. https://doi.org/10.1029/2021JF006066

Nordstrom, K. F. (1980). Cyclic and Seasonal Beach Response: A Comparison of Oceanside and Bayside Beaches. *Physical Geography*, *1*(2), 177–196. https://doi.org/10.1080/02723646.1980.10642199

O'Donnell, S. J., Schneider, M. K., Rittschof, D., & Reinsel, K. (2003). Spatial and predation ecology of whelks in a shallow embayment in the Rachel Carson reserve, Beaufort, North Carolina.(Environmental Poster Session 10: 00 AM-11: 00 AM). *The Ohio Journal of Science*, *103*(1), A-12.

Paerl, H. W., Hall, N. S., Hounshell, A. G., Luettich, R. A., Rossignol, K. L., Osburn, C. L., & Bales, J. (2019). Recent increase in catastrophic tropical cyclone flooding in coastal North Carolina, USA: Long-term observations suggest a regime shift. *Scientific Reports*, *9*(1), 10620. https://doi.org/10.1038/s41598-019-46928-9

Park, J.-Y., & Wells, J. T. (2007). Spit Growth and Downdrift Erosion: Results of Longshore Transport Modeling and Morphologic Analysis at the Cape Lookout Cuspate Foreland. *Journal of Coastal Research*, *23*(3 (233)), 553–568. https://doi.org/10.2112/03-0116.1

Pennings, S. C., and Bertness, M. D. (2001). Salt marsh communities. *Marine Community Ecology*, 289–316.

Penland, S., Suter, J. R., & Boyd, R. (1985). Barrier island arcs along abandoned Mississippi River deltas. *Marine Geology*, *63*(1), 197–233. https://doi.org/10.1016/0025-3227(85)90084-2

Pilkey, O. H., Cooper, J. A. G., & Lewis, D. A. (2009). Global Distribution and Geomorphology of Fetch-Limited Barrier Islands. *Journal of Coastal Research*, *25*(4), 819–929.

Poling, D. and Johnston, D. W. (2023). Drones and Machine Learning for Marine Animal Behavior Analysis. Master's project, Duke University. https://hdl.handle.net/10161/27232

Portos-Amill, L., Nienhuis, J. H., & de Swart, H. E. (2023). Gradual Inlet Expansion and Barrier Drowning Under Most Sea Level Rise Scenarios. *Journal of Geophysical Research: Earth Surface*, *128*(11), e2022JF007010. https://doi.org/10.1029/2022JF007010

Puckett, B., Falvo, C., Deaton, C., Morse, B., Smith, E., & Ridge, J. *A Protocol for Monitoring Coastal Wetlands with Drones: Image Acquisition, Processing, and Analysis Workflows*.

Ratliff, K. M., & Murray, A. B. (2014). Modes and emergent time scales of embayed beach dynamics. *Geophysical Research Letters*, *41*(20), 7270–7275. https://doi.org/10.1002/2014GL061680

Ridge, J. T., Gray, P. C., Windle, A. E., & Johnston, D. W. (2020). Deep learning for coastal resource conservation: Automating detection of shellfish reefs. *Remote Sensing in Ecology and Conservation*, *6*(4), 431–440. https://doi.org/10.1002/rse2.134

Riggs, S. R., & Ames, D. V. (2007). Effect of storms on barrier island dynamics, Core Banks, Cape Lookout National Seashore, North Carolina, 1960-2001. In *Scientific Investigations Report* (2006–5309). U.S. Geological Survey. https://doi.org/10.3133/sir20065309

Robinson, M. M., & McBride, R. (2003). *Geomorphic evolution and geology of Old Currituck Inlet and its flood tidal delta, Virginia/North Carolina, USA (Part I)*. International Conference on Coastal Sediments 2003.

Rodriguez, A. B., Duran, D. M., Mattheus, C. R., & Anderson, J. B. (2008). Sediment accommodation control on estuarine evolution: An example from Weeks Bay, Alabama, USA. *Special Paper of the Geological Society of America*, *443*, 31–42. https://doi.org/10.1130/2008.2443(03)

Rodriguez, A. B., Fegley, S. R., Ridge, J. T., VanDusen, B. M., & Anderson, N. (2013). Contribution of aeolian sand to backbarrier marsh sedimentation. *Estuarine, Coastal and Shelf Science*, *117*, 248–259. https://doi.org/10.1016/j.ecss.2012.12.001

Selby, L. (2020). *Human Dimensions of Wild Horse Management: Visitor Attitudes and Behaviors on North Carolina's Barrier Islands*.

Seymour, A. C., Ridge, J. T., Rodriguez, A. B., Newton, E., Dale, J., & Johnston, D. W. (2018). Deploying Fixed Wing Unoccupied Aerial Systems (UAS) for Coastal Morphology Assessment and Management. *Journal of Coastal Research*, *34*(3), 704. https://doi.org/10.2112/JCOASTRES-D-17-00088.1

Seymour, A. C., Ridge, J. T., Newton, E., Rodriguez, A. B., & Johnston, D. W. (2019). Geomorphic response of inlet barrier islands to storms. *Geomorphology*, *339*, 127–140. https://doi.org/10.1016/j.geomorph.2019.04.021

Shepard, C. C., Crain, C. M., & Beck, M. W. (2011). The Protective Role of Coastal Marshes: A Systematic Review and Meta-analysis. *PLOS ONE*, *6*(11), e27374. https://doi.org/10.1371/journal.pone.0027374

Shih, S.-M., & Komar, P. D. (1994). Sediments, Beach Morphology and Sea Cliff Erosion within an Oregon Coast Littoral Cell. *Journal of Coastal Research*, *10*(1), 144–157.

Sirianni, H., Sirianni, M. J., Mallinson, D. J., Lindquist, N. L., Valdes-Weaver, L. M., Moody, M., Henry, B., Colli, C., Rubino, B., Peñalver, M. M., & Henne, C. (2022). Quantifying Recent Storm-Induced

Change on a Small Fetch-Limited Barrier Island along North Carolina's Crystal Coast Using Aerial Imagery and LiDAR. *Coasts*, *2*(4), Article 4. https://doi.org/10.3390/coasts2040015

Smith, J. B., & FitzGerald, D. M. (1994). Sediment Transport Patterns at the Essex River Inlet Ebb-Tidal Delta, Massachusetts, U.S.A. *Journal of Coastal Research*, *10*(3), 752–774.

Smith, Q. H. T., Heap, A. D., & Nichol, S. L. (2010). Origin and Formation of an Estuarine Barrier Island, Tapora Island, New Zealand. *Journal of Coastal Research*, *26*(2), 292–300.

Stutz, M. L., & Pilkey, O. H. (2011). Open-Ocean Barrier Islands: Global Influence of Climatic, Oceanographic, and Depositional Settings. *Journal of Coastal Research*, *27*(2), 207–222. https://doi.org/10.2112/09-1190.1

Suanez, S., Cariolet, J.-M., Cancouët, R., Ardhuin, F., & Delacourt, C. (2012). Dune recovery after storm erosion on a high-energy beach: Vougot Beach, Brittany (France). *Geomorphology*, *139–140*, 16–33. https://doi.org/10.1016/j.geomorph.2011.10.014

Taggart, J. B. (2008). Management of feral horses at the North Carolina National Estuarine Research Reserve. *Natural Areas Journal*, *28*(2), 187–195.

Taggart, J. B. and K. Henderson (1988). A field guide to exploring the North Carolina National Estuarine Research Reserve. Division of Coastal Management, North Carolina Department of Natural Resources and Community Development. Raleigh, NC.

Temmerman, S., Meire, P., Bouma, T. J., Herman, P. M., Ysebaert, T., & De Vriend, H. J. (2013). Ecosystem-based coastal defence in the face of global change. *Nature*, *504*(7478), 79–83.

Theuerkauf, E. J., Rodriguez, A. B., Fegley, S. R., & Luettich Jr., R. A. (2014). Sea level anomalies exacerbate beach erosion. *Geophysical Research Letters*, *41*(14), 5139–5147. https://doi.org/10.1002/2014GL060544

Thompson, J. A., Zinnert, J. C., & Young, D. R. (2017). Immediate effects of microclimate modification enhance native shrub encroachment. *Ecosphere*, *8*(2), e01687. https://doi.org/10.1002/ecs2.1687

Turki, I., Medina, R., González, M., & Coco, G. (2013). Natural variability of shoreline position: Observations at three pocket beaches. *Marine Geology*, *338*, 76–89. https://doi.org/10.1016/j.margeo.2012.10.007

Valle-Levinson, A., Dutton, A., & Martin, J. B. (2017). Spatial and temporal variability of sea level rise hot spots over the eastern United States. *Geophysical Research Letters*, *44*(15), 7876–7882. https://doi.org/10.1002/2017GL073926

Walters, D. C., & Kirwan, M. L. (2016). Optimal hurricane overwash thickness for maximizing marsh resilience to sea level rise. *Ecology and Evolution*, *6*(9), 2948–2956. https://doi.org/10.1002/ece3.2024

Walters, D., Moore, L. J., Duran Vinent, O., Fagherazzi, S., & Mariotti, G. (2014). Interactions between barrier islands and backbarrier marshes affect island system response to sea level rise: Insights

from a coupled model. *Journal of Geophysical Research: Earth Surface*, *119*(9), 2013–2031. https://doi.org/10.1002/2014JF003091

White, S. A., & Wang, Y. (2003). Utilizing DEMs derived from LIDAR data to analyze morphologic change in the North Carolina coastline. *Remote Sensing of Environment*, *85*(1), 39–47. https://doi.org/10.1016/S0034-4257(02)00185-2

Wilson, M. D., Watts, B. D., & LeClerc, J. E. (2007). Assessing habitat stability for disturbance-prone species by evaluating landscape dynamics along the Virginia barrier islands. Center for Conservation Biology Technical Report Series. College of William and Mary.

Young, D. R., Porter, J. H., Bachmann, C. M., Shao, G., Fusina, R. A., Bowles, J. H., Korwan, D., & Donato, T. F. (2007). Cross-scale patterns in shrub thicket dynamics in the Virginia barrier complex. *Ecosystems*, *10*, 854–863.

Zhang, K., Liu, H., Li, Y., Xu, H., Shen, J., Rhome, J., & Smith III, T. J. (2012). The role of mangroves in attenuating storm surges. *Estuarine, Coastal and Shelf Science*, *102*, 11–23.

Zinnert, J. C., Shiflett, S. A., Via, S., Bissett, S., Dows, B., Manley, P., & Young, D. R. (2016). Spatial–Temporal Dynamics in Barrier Island Upland Vegetation: The Overlooked Coastal Landscape. *Ecosystems*, *19*(4), 685–697. https://doi.org/10.1007/s10021-016-9961-6

Zinnert, J. C., Stallins, J. A., Brantley, S. T., & Young, D. R. (2017). Crossing Scales: The Complexity of Barrier-Island Processes for Predicting Future Change. *BioScience*, *67*(1), 39–52. https://doi.org/10.1093/biosci/biw154

Zinnert, J. C., Via, S. M., Nettleton, B. P., Tuley, P. A., Moore, L. J., & Stallins, J. A. (2019). Connectivity in coastal systems: Barrier island vegetation influences upland migration in a changing climate. *Global Change Biology*, *25*(7), 2419–2430. https://doi.org/10.1111/gcb.14635